Universität Hamburg
DER FORSCHUNG | DER LEHRE | DER BILDUNG

Bachelor's Thesis

Long-Lived Axion-Like Particles at the Future Circular Electron-Positron Collider

submitted by
Elnura Bakhishova

University of Hamburg
Faculty for Mathematics, Informatics and Natural Sciences
Department of Physics

2025

Matr.-Nr.: 7508151
First Supervisor: Prof. Dr. Freya Blekman
Second Supervisor: Dr. Juliette Alimena

Contents

Abstract

As the leading theory in particle physics, the Standard Model (SM) defines our understanding of the subatomic world. However, observed phenomena have proven that the SM, despite its great success, is not complete yet and the search for particles Beyond the Standard Model (BSM) has surged ever since. In models that try to address the problems of the SM, BSM long-lived particles (LLPs), which have longer lifetimes than unstable SM particles, occur naturally. With a proposed circular electron-positron collider, the FCC-ee, these BSM LLPs could be discovered.

This thesis focuses specifically on the production and detection of long-lived axion-like particles (ALPs), which are well-motivated BSM particles and also possible dark matter candidates. Utilizing the $e^+e^- \to Z \to a\gamma \to \gamma\gamma\gamma$ channel, which only depends on the ALP-photon coupling $c_{\gamma\gamma}$ under certain assumptions, the sensitivity of the FCC-ee to detect ALPs is examined. Employing the analysis framework of the Future Circular Collider (FCC), the simulation and analysis of events for ALP production were conducted, testing coupling constants ranging from 10^{-6} to 1.6 and ALP masses between 0.01 GeV and 30 GeV. Finally, the sensitivity of the FCC-ee to a long-lived ALP signature is studied for various settings of the ALP parameters.

1 Introduction

The particle standing at the center of this thesis is the axion-like particle (ALP), a hypothetical neutral particle originating in some theories beyond the Standard Model (BSM). ALPs are predicted by models that address the strong Charge-Parity (CP) problem and can exhibit a wide range of masses and couplings to the Standard Model (SM) [1]. Due to their rather weak coupling to SM particles, ALPs can be long-lived. This characteristic is of great importance for experimental detection since long-lived particles (LLPs) have special signatures. While most particles produced in high-energy physics experiments decay almost instantaneously, LLPs can travel measurable distances from their initial creation point before they decay into other particles.

LLPs are difficult to detect with the typical trigger and reconstruction techniques used in high-energy experiments at hadron colliders. The Future Circular Collider (FCC), which is proposed to be built at CERN, would become the world's largest particle collider and would reach world-record luminosities [2]. The FCC would allow us to probe BSM scenarios further and study BSM LLPs, potentially leading to discoveries. The first stage of the FCC, which contains electron-positron collisions (FCC-ee), would also allow for more precise measurements of fundamental parameters of the SM and for increased sensitivity to new particles due to its cleaner environment [3].

This thesis is concerned with the first stage of the FCC, the FCC-ee. Computational tools are used to create realistic simulations of a specific ALP production channel, followed by the analysis of generated events within the preexisting analysis framework of the FCC. The goal is to further investigate the properties of ALPs and the underlying physics of the simulation by varying the ALP mass and coupling constant. Additionally, selected background events will be examined and event selections will be made to reduce the amount of background, thereby increasing the sensitivity for ALP signal detection at the FCC-ee.

1.1 The Future Circular electron-positron Collider

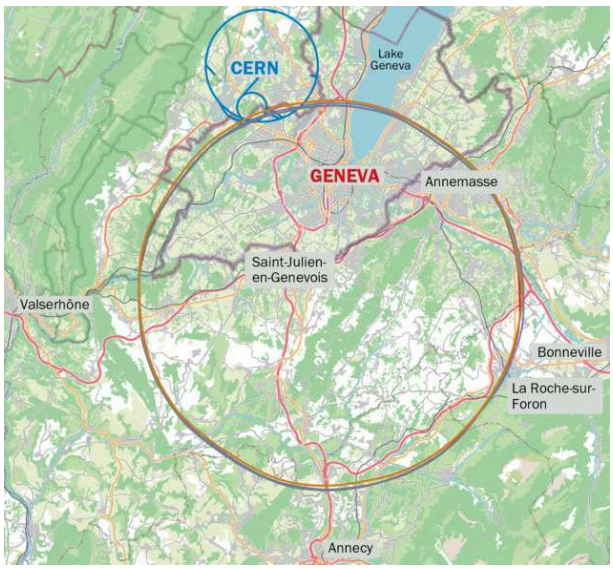

Figure 1: Comparison of the current largest particle collider, the LHC (blue), with the proposed FCC (orange). The FCC's circumference is 90.7 km, which is over three times bigger than that of the LHC's [4].

Currently, the Large Hadron Collider (LHC) at the "Conseil Européen pour la Recherche Nucléaire" (CERN) is the world's largest and highest-energy particle accelerator with a circumference of 27 km and a record center-of-mass energy of 13.6 TeV. The collider has brought valuable scientific breakthroughs, such as the discovery of the Higgs boson in 2012 as the last missing piece of the SM puzzle.

To explore possibilities beyond the current framework of the visible sector, the proposed CERN high-energy lepton collider, the FCC-ee, plays a crucial role. In the FCC's first stage, electron-positron collisions will be initiated at center-of-mass energies ranging from the Z-pole (91 GeV), through the WW (160 GeV) threshold, to the top-quark pair-production threshold of 365 GeV. The Z-pole run is spread over three different center-of-mass energies (40 ab-1 at 87.9 GeV, 40 ab-1 at 94.3 GeV, 125 ab-1 at 91.2 GeV, for a total of about $6 \cdot 10^{12}$ Z-bosons) [5].

With a circumference of 90.7 km - over three times that of the LHC - the FCC would be the world's largest collider (see Figure 1), reaching new world-record luminosities. The potential instantaneous luminosities for the FCC-ee are depicted in Figure 2 as a function of the center-of-mass energy, starting from 88 GeV and going up to 365 GeV. According to the latest updates from 2024, the FCC-ee baseline is now with four interaction points [6], which results in a gain in luminosity (see Figure 2). The collider will run for four years around the Z boson resonance, accumulating an integrated luminosity of $205ab^{-1}$ for the Z-pole run [5] and a total of $6 \cdot 10^{12}$ Z bosons available for study [6]. The large amount of Z bosons will allow for high-accuracy measurements of electroweak parameters mainly limited by systematic uncertainties.

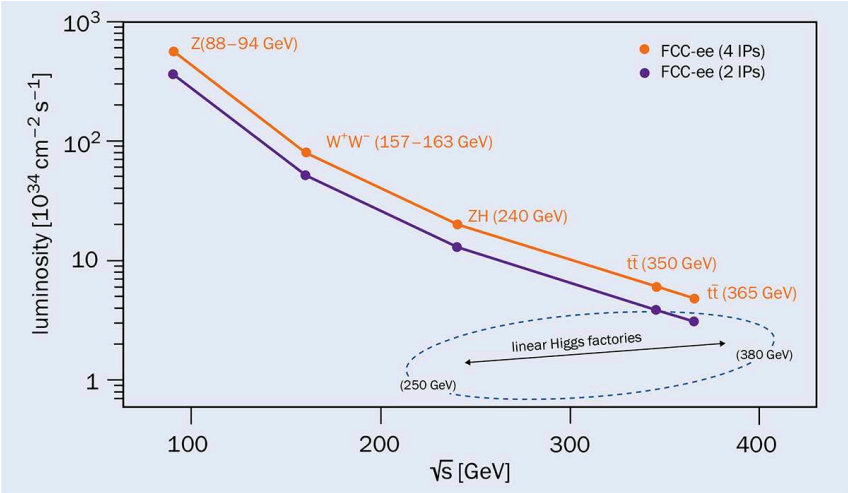

Figure 2: Instantaneous luminosity versus center-of-mass energy for the FCC-ee for four (orange) and for two (purple) interaction points. For comparison, the typical luminosity of linear colliders with one interaction point is also shown [7].

Electron-positron collisions are excellent for precision measurements because they provide a "clean" environment to measure the products of the collision. "Clean" in this case means that fewer particles are produced in the collision and the background is less cluttered compared to proton-proton collisions. The total momentum and energy are well-defined, as electrons and positrons are elementary particles with no substructure, unlike protons. This simplifies theoretical calculations and the interpretation of collision results. Most importantly, the clean environment, combined with the high luminosity, allows us to reduce uncertainties and increases the sensitivity to new physics lying below the weak scale [3]. This includes weakly coupled particles from the dark sector and other candidates for BSM physics. In particular, for this thesis, the FCC-ee's unprecedented potential for new particle searches will be investigated, specifically in the context of LLPs and ALPs. More on the properties of these particles and their detection in the FCC-ee will be covered in Section 2.

The e^+e^- stage of the FCC will also provide precision measurements of fundamental parameters of the SM. Thorough precision tests of the strong, weak, and electromagnetic coupling constants will be made with uncertainties reduced by up to two orders of magnitude [3]. Also, during the Z-pole run, properties of the Higgs boson, the electroweak gauge bosons, and the top quark will be investigated with so far unreached levels of precision.

After the e^+e^- run, the infrastructure is proposed to be reused for the FCC-hh stage. Here, proton-proton collisions will take place in the 90.7 km long tunnel of the FCC, which accelerates the charged hadrons close to the speed of light. The final goal will be to achieve 100 TeV proton-proton collisions, far beyond the energy scale of the LHC. The record center-of-mass energy of the FCC-hh, which is seven times that of the LHC, expands the direct discovery reach for new particles [7].

The FCC-ee will be able to probe regions not accessible to the LHC and has excellent

potential for direct searches for ALPs with masses up to 90 GeV [3].
The FCC is an ambitious future project expected to deliver highly significant scientific results. The FCC feasibility study, which investigates the technical, financial, geological, and environmental feasibility of the project, is scheduled for completion in 2025. Discussions regarding its potential construction are ongoing, with a final decision by CERN member states and international partners expected by 2028. If approved, construction will commence in the 2030s. The FCC-ee is planned to begin operations in the mid-2040s and run for approximately 15 years before transitioning to the FCC-hh stage [2].

1.2 The IDEA detector

To successfully operate the world's most powerful particle collider and to utilize it to its full potential, appropriately advanced detectors will be needed. Three detector design concepts have been proposed for the FCC-ee: the "CLIC-like Detector" (CLD), the "Innovative Detector for Electron-positron Accelerators" (IDEA), and the noble-liquid based "Lepton-Lepton collider Experiment with Granular Read-Out" (ALLEGRO) [8] [9]. The analysis conducted in this thesis uses the IDEA detector, which would provide high-resolution energy measurements and excellent particle identification.

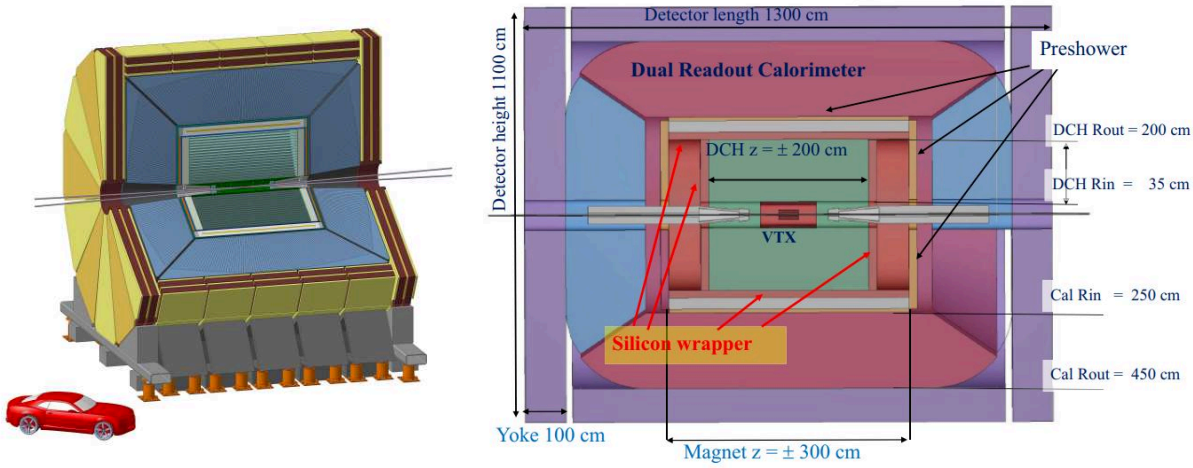

(a) (b)

Figure 3: Schematics of the IDEA detector concept proposed for the FCC-ee. (a) shows a 3D view and (b) shows a more detailed cross section view of the detector layout. The innermost part is a silicon pixel vertex detector (VTX), followed by a large-volume drift wire chamber (DCH) that is surrounded by a silicon wrapper layer, a solenoid coil, a pre-shower detector, a dual-readout calorimeter, a muon chamber, and a magnetic yoke. [8][10].

Figure 3 shows the conceptual design for the IDEA detector consisting of multiple subdetectors. The IDEA vertex detector (VTX) is a silicon pixel detector around the 1.5 cm radius beam pipe, in the direct vicinity of the particle collision point, and detects the tracks of charged particles with an excellent resolution of approximately $3\mu m$ [3].

Particles with short decay vertices can be detected there. After the VTX, the next closest component to the beamline is a large-volume cylindrical short-drift chamber, the DHC. It has high transparency in terms of radiation lengths [10] and enables precise momentum measurements due to its good spatial resolution of $< 100\mu m$ using cluster counting. Consequently, this leads to improved particle identification.
The silicon wrapper layer around the DHC consists of silicon micro-strip detectors and provides additional accurate momentum measurements and track reconstruction.
The solenoid magnet surrounding the tracking system creates a magnetic field of two Tesla, which bends the path of the charged particles.
The next layer, the IDEA pre-shower detector, identifies the particles and is followed by a dual readout calorimeter, which detects the deposited energies of the electromagnetic and hadronic showers, matching the tracks to the pre-shower signals. While the electromagnetic calorimeter detects electrons and photons, the hadronic calorimeter detects hadrons, such as protons.
The flux return yoke, which contains the magnetic flux, and the muon chambers make up the outermost part of the detector.
The geometric dimensions of the detector are given in Figure 3(b). The VTX ranges from 1.7 cm to 34 cm in the radial direction. The drift chamber expands from 35 cm to 2 m with an additional 0.5 m for the solenoid coil, 2 m for the calorimeter, and 1 m for the flux return yoke, giving a total radial length of 5.5 m for IDEA.
For a general illustration of the angles and the coordinate system of a detector, see Figure 4.

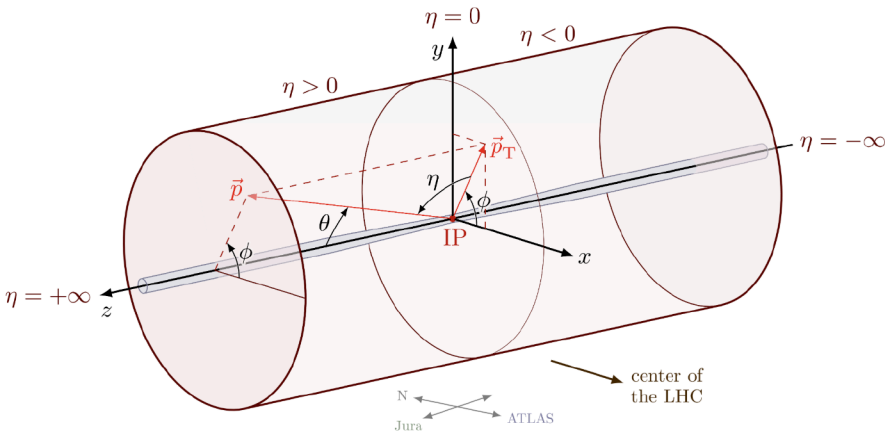

Figure 4: Graphical illustration of the 3D coordinate system at the CMS detector to depict the pseudorapidity η and the azimuthal angle ϕ [11].

1.3 Detection of long-lived particles at the FCC

As the FCC-ee will venture further into search territories beyond the SM, looking, for example, for BSM LLPs, that factor must be considered in the detector design. Long-lived particles travel measurable distances from where they are produced. If they decay within the detector, their displaced decay products could be measured. Furthermore, if LLPs decay into charged particles within the detector, they will also produce displaced vertices. To study these signatures, dedicated techniques are needed.
In order to measure displaced particles and displaced vertices, it is essential to provide a large detector volume.
If the displaced vertex of the LLP is inside the detector, the resulting signature, of e.g. a long-lived ALP, can be reconstructed with high efficiency since the signature is often almost background-free. LLPs that decay outside of the detector, due to low mass or weak coupling, could be detected through missing-energy signatures or by future detectors specifically designed to search for long-lived particles [12].
The sensitivity to long-lived ALPs in the FCC-ee with the IDEA detector will be explored in the analysis presented here.

2 Theory

In this section, the key physical foundations, essential to understanding the motivation and nature of ALPs, are discussed. This includes an introduction to BSM physics and a closer look at an example signal process for ALP production and decay.

2.1 Phenomena beyond the Standard Model

There are gravitational effects that cannot be explained by visible matter alone. By observing different spiral galaxies, Rubin and Ford delivered evidence in the 1970s that stars in the outer region of galaxies move faster around their galaxy center than the matter we see could account for. It was deduced that there must be some invisible matter that creates enough gravity to hold the galaxies together: dark matter (DM) [13] [14]. The matter that we know, elementary particles from the standard model of particle physics, only makes up 5% of our universe, while dark matter and dark energy make up 25% and 70% each, showing that there is a big part of the universe that we cannot see and understand yet. Dark energy is a mysterious force that was introduced to describe the acceleration of the universe's expansion. While dark energy pushes galaxies apart, DM pulls them together. It is still unknown what DM is exactly and whether it can interact with particles of the SM through means other than gravitation. Accordingly, numerous experiments have been proposed and conducted in an attempt to answer this question. The search for DM encompasses a broad landscape of mass scale ($\sim$ meV-ZeV) and coupling strength ($\sim 1 - 10^{-12}$ or less) to the SM [7].

Of great importance for the theoretical foundation of this thesis is the BSM phenomena of Charge-Parity (CP) violation because that is what motivated the introduction of axions, and by extension, ALPs. In physics CPT (Charge conjugation, Parity, Time) invariance is believed to uphold for all interactions, meaning that all quantum field theories are symmetric under the combined transformation of charge, parity, and time. However, under CP transformation, the physics of particles does not always remain equal. In 1964, Cronin and Fitch delivered evidence for CP violation in the decay of neutral K-mesons [15], proving that there is a CP-symmetry violation for the electroweak theory. This led to the famous and still unsolved strong CP problem, which deals with the question of why violation of the CP-symmetry for quantum chromodynamics (QCD) has not been observed yet. Since the CP violation solely from electroweak interaction alone would not be enough to explain the baryon asymmetry of the universe, it is expected that QCD is also contributing to the CP-asymmetry. Additionally, according to the QCD Lagrangian, it should be possible for the CP-symmetry to be broken [16].

As a solution for the problem, new pseudoscalar particles, namely axions, were introduced as part of the Peccei-Quinn mechanism, a suggested theory to address the strong CP problem. ALPs are generally used for theories with a spontaneously broken global

symmetry [16].

2.2 Long-lived particles

LLPs are BSM particles with a shorter decay width and a longer lifetime than unstable SM particles. While most particles produced in high-energy physics experiments decay almost instantaneously, LLPs can travel macroscopic distances from their initial creation point before they decay into other particles. As a result, they exhibit displaced vertices, which can be identified as a visible displacement of the track in a detector, or, if the LLP decays outside of the detector volume, missing energy will be detected. The distinct signature of the hypothesized LLPs could be detected in the proposed FCC [1]. BSM particles that can acquire long lifetimes are, for example, ALPs and heavy neutral leptons. The existence of LLPs is of particular interest for modern particle physics, since they point to physics BSM, answering unsolved questions of the current model mentioned in Section 2.1.

There are two main factors that can make a particle long-lived: a weak coupling constant and a low mass. A weak coupling reduces the probability of interaction and a smaller mass limits the number of possible decay channels. These two properties of LLPs have a significant influence on the particle's characteristics and will therefore be of particular interest for the analysis of long-lived ALPs conducted in this thesis.

2.3 Axion-like particles

ALPs were motivated by the strong CP problem and are hypothesized pseudoscalar, light, neutral, spin-zero bosons, which are odd under CP transformation. They can be understood as a generalization of the axion. For ALPs, unlike axions, mass and coupling strength are independent parameters, leaving freedom for the expected phenomenology [17]. These parameters are not set and can vary within a big range. The detection of ALPs would confirm the Peccei-Quinn mechanism and would explain the baryon asymmetry of the universe.

Furthermore, ALPs could be candidates for non-thermal dark matter in certain ranges of the parameter space of mass and coupling or mediators to a dark sector [1].

2.3.1 ALP production and decay

This section takes a quick dive into the potential interactions between ALPs and SM particles if such interactions exist.

The hypothesized ALP couples to SM particles with dimension-5 operators. The specific coupling to the Z boson and to photons is possible in the broken phase of the electroweak

symmetry and is described by the following terms in the Lagrangian [18]:

$$\mathcal{L}_{\text{eff}} \ni e^2 c_{\gamma\gamma} \frac{a}{\Lambda} F_{\mu\nu} \tilde{F}^{\mu\nu} + \frac{2e^2}{s_w c_w} c_{\gamma Z} \frac{a}{\Lambda} F_{\mu\nu} \tilde{Z}^{\mu\nu} + \frac{e^2}{s_w^2 c_w^2} c_{ZZ} \frac{a}{\Lambda} Z_{\mu\nu} \tilde{Z}^{\mu\nu}. \tag{1}$$

The new-physics scale Λ is related to the axion decay constant f_a via $\Lambda = 32\pi^2 f_a |c_{GG}|$, and "a" stands for the pseudoscalar ALP field. $F_{\mu\nu}$ and $Z_{\mu\nu}$ are field-strength tensors describing photons and Z bosons. The coupling constants are described by the Wilson-coefficients $c_{\gamma\gamma}$, $c_{\gamma Z}$ and c_{ZZ}.
ALP decays into gauge bosons, leptons, and quarks are possible. The relevant ALP decay width for this thesis is [19]

$$\Gamma(a \to \gamma\gamma) = \frac{\alpha^2 m_a^3}{64\pi^3 f^2} c_{\gamma\gamma}^2, \tag{2}$$

where the ALP decays into two photons, as will be further explained in Section 2.4. The decay width scales with the third power of the ALP mass m_a and taking into consideration the formula for the calculation of lifetimes,

$$\tau = \frac{\hbar}{\Gamma}, \tag{3}$$

it can be deduced that the smaller the ALP mass is, the more long-lived the particle is. Similarly, a smaller coupling constant $c_{\gamma\gamma}$ leads to greater lifetimes.

2.4 Signal process

There are many potential ways for the production of the hypothesized ALP. However, in the scope of this thesis, only one particular process will be of interest for the event production and analysis. This particular process produces an ALP in association with a Z boson in the following way:

$$e^+e^- \to Z \to a\gamma \to \gamma\gamma\gamma, \tag{4}$$

where $a \to \gamma\gamma$.
During the Z-pole run of the FCC-ee, an electron-positron collision would very likely produce a Z boson. In the signal process of interest, the Z boson then decays into a photon and an ALP, which then decays into two further photons, leaving us with three photons in the final state, as illustrated in Figure 5.
One advantage of the $e^+e^- \to Z \to a\gamma \to \gamma\gamma\gamma$ channel over other processes is that it only depends on one coupling (under the assumption that the coupling originates from U(1) gauge bosons before electroweak symmetry breaking [19]). The relevant coupling for the channel is the ALP-photon coupling $c_{\gamma\gamma}$. Therefore, for the analysis, all other couplings are set to zero to ensure a branching ratio of 1 for the ALP-to-photon decay. Setting all

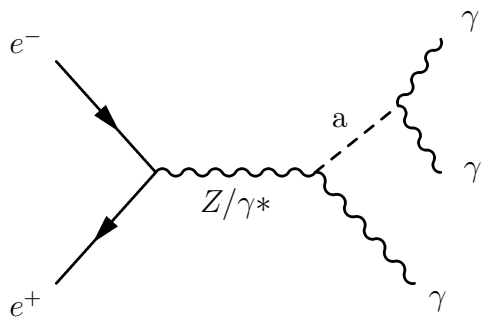

Figure 5: Feynman diagram of the generated process for the ALP production. The ALP is produced in association with a Z boson and decays into two photons.

the other couplings to zero allows the ALP to become long-lived due to fewer possibilities for it to decay.

3 Methodology

As the FCC is still undergoing feasibility studies and does not exist yet, there are no experimental data available for the analysis of possible ALP production. Instead, various software and computational tools are used to create realistic simulations of the desired signal event and to simulate the detector response of IDEA. The analysis of generated events follows within the preexisting analysis framework of the Future Circular Collider[1], allowing one to define and calculate variables of the particles, to make selections, and to display results in the form of histograms.
An overview of the entire process is depicted in Figure 6 and will be further elaborated in the following subsections, where the software setup will be explained [20].

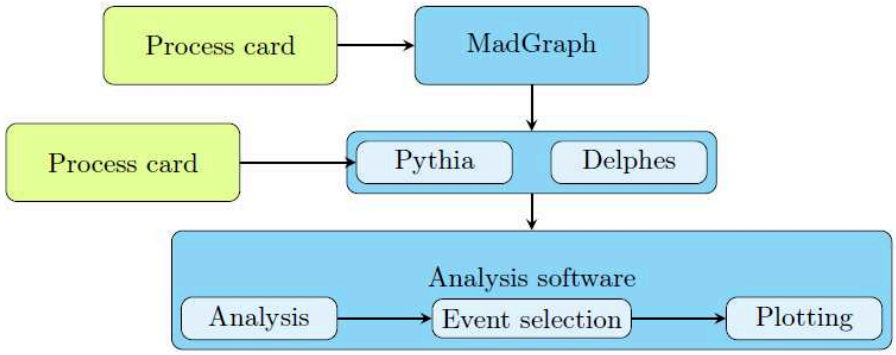

Figure 6: Overview of the generation and analysis of particle collision events with the corresponding computational tools. Events are first generated with MadGraph and then simulated with the programs Pythia and Delphes [20].

The following properties were set for the simulation and analysis:

- Integrated luminosity $\mathcal{L} = 205ab^{-1}$
- Center-of-mass energy: $\sqrt{s} = 91$ GeV
- Axion decay constant $f_a = 6.33$ GeV
- ALP mass: 0.01 GeV$\leq m \leq$ 30 GeV
- All couplings set to 0 except for $c_{\gamma\gamma}$: $10^{-6} \leq c_{\gamma\gamma} \leq$1.6

3.1 Simulation

To generate the desired particle collision data, several steps must be carried out using three different programs. Firstly, matrix elements are calculated and Monte Carlo generated events are produced with $MadGraph5\_aMC@NLO\,v.3.5.6$ [21]. For this, a MadGraph

[1]The Common analysis framework for the Future Circular Collider: https://hep-fcc.github.io/FCCAnalyses/

process card with specified configurations for the properties of the signal or background is used as input. An example of a MadGraph process card used for the generation of an ALP can be found in Appendix B.
The relevant signal process for the ALP production and decay is the signature event discussed in Section 2.4. In previous work, samples for the same signal event were created [22]. Within the scope of this thesis, new samples were generated to increase the number of generated events and to update the data format to match the latest software developments. Different ALP masses and coupling strengths were applied for the configuration of the MadGraph process cards. For the simulation of the signal event, all couplings were set to zero except for the coupling to photons $c_{\gamma\gamma}$, which is varied between values from 10^{-6} to 1.6, while the ALP mass is varied between 0.01 GeV and 30 GeV.
The output files from MadGraph (.lhe files) are used as the input for the next step, where the programs Pythia 8 and Delphes run simultaneously [23] [24].
Pythia takes a process card as input specifying the collision properties. An example of the Pythia process card is shown in Appendix C.
Pythia simulates the electromagnetic showering processes and hadronization. Delphes uses the IDEA detector card to perform reconstructions and to imitate the detector response [25].

3.2 Analysis within the "FCCAnalyses" framework

For the majority of FCC-related analyses, the common analysis framework "FCCAnalyses" is used. The analysis input files contain physics objects in EDM4hep format and the main event processor for the analysis is based on RDataFrame [26]. The simulation analysis is executed with ROOT and C++-based scripts, which are called in corresponding Python scripts.
A simplified overview of the process is depicted in Figure 7. Firstly, the accessor functions are declared and defined in C++ header (.h) and source (.cc) files. The accessor functions are then used in the "Stage 1" Python script to define and access desired variables of the EDM4hep objects. This creates a column in the RDataFrame and fills it with the return value of the accessor function. Following this, the next stage "Final" is used to define the parameters for the plots and, more importantly, to make event selections to reduce background signals. The last Python script "Plots" is used to plot histograms of the processed data.

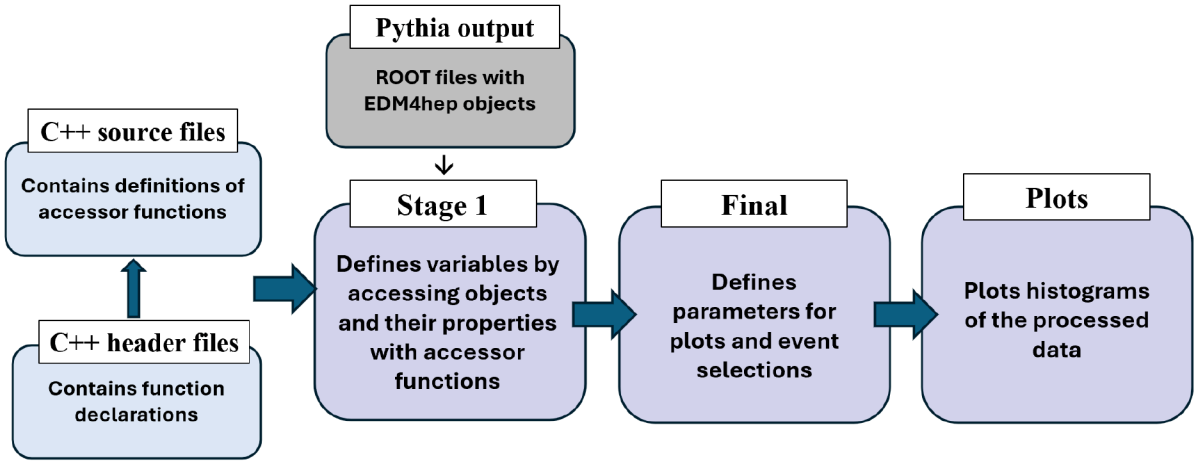

Figure 7: Simplified overview of the analysis steps in the FCCAnalyses framework.

3.3 Scaling and normalization

In order to estimate the number of expected events during the Z-pole run at the FCC-ee, a scaling to cross section σ and integrated luminosity $\mathcal{L}_{int}$ can be applied with the equation

$$N_{exp} = \sigma \mathcal{L}_{int} \,, \tag{5}$$

where N_{exp} is the expected number of events. For scaling after event selection, the following equation is used:

$$N_{exp} = \sigma \mathcal{L}_{int} \frac{N_{sel}}{N_{tot}}, \tag{6}$$

where N_{tot} is the total number of events before any selections and N_{sel} is the remaining number of events after selections were made.

To take into account that the Z-pole run is spread over three different center-of-mass energies (see Section 1.1) the number of expected events N_{exp} needs to be multiplied with a factor of 0.49 for the signal and for resonant Z backgrounds, as was decided in a recent FCC Physics and Performance BSM Working Group Meeting [27]. This factor corrects for an overestimation of the expected number of events.

Sometimes, the plots in this thesis are normalized to unit area instead of to the expected number of events. This allows for direct comparison of the shapes of different signal and background distributions, regardless of their cross section. It facilitates the comparison of the histogram shapes and thereby also the physical properties of the different process samples. For this analysis, the scaling for background events was implemented in a way that the sum of the stacked backgrounds fulfill the normalization to unit area.

4 Analysis

This section will discuss the outcomes of the particle collision simulation. Histograms of relevant variables highlighting different physical behaviors of background and signal have been plotted and analyzed. This comparison was then used to make selections on the events to reduce the relative amount of background events compared to signal events.
It is important to note that the histograms in this thesis are either labeled with "gen" or with "reco" followed by a variable name. Histograms that are labeled with "gen" are generated events coming straight from the simulation with MadGraph and Pythia, without factoring in the properties of the detector. Events labeled with "reco" correspond to the reconstruction with the IDEA detector, using the detector simulation software Delphes. The reconstruction takes measurement errors and misidentification of particles into account, which ultimately leads to more realistic simulations. For all signal and background samples in this analysis, 10^6 events were generated.

4.1 Signal

To understand the physical behavior of the ALP and to analyze its sensitivity to detection for diverse scenarios, several signal points were generated. The $e^+e^- \to Z \to a\gamma \to \gamma\gamma\gamma$ process was generated, as described in Section 2.4. The signal points encompass eight different masses ranging from 0.01 GeV to 30 GeV and twelve different coupling constants ranging from 10^{-6} to 1.6 (see Table in Appendix A for a full list of all created samples). For demonstration purposes, the plots will illustrate only a few chosen signal points.
Firstly, it needs to be understood how different ALP masses and couplings influence the process cross section. Generally, the cross section increases for bigger coupling strengths $c_{\gamma\gamma}$ (see Table 1) because the ALP is then more likely to couple to photons, increasing the production of the process. For larger masses, the cross section decreases because a heavier ALP reduces the available energy for the photon and leaves less room in the phase space. That behavior can also be seen in Table 1. According to Equation 5, a bigger cross section for a certain process results in a larger number of expected events. These processes are easier to detect than the ones with smaller cross sections if no backgrounds and selections are considered.
Now, with the knowledge of the previous sections, the signal events can be studied in detail by analyzing the histograms for different variables. The goal here is to find variables to distinguish the signal from background events. One of the most important traits of the process discussed in this thesis is the three final state photons, where one photon is decaying directly from the Z-boson and the other two are decaying from a displaced vertex from the ALP (see Figure 5). The number of generated ("gen") and reconstructed ("reco") final state photons for various choices of ALP parameters is shown in Figure 8. The plots shown in this section are scaled to the expected number of events during the Z-

m_a[GeV]	$c_{\gamma\gamma}$	σ[pb]
10	1.6	6.764
0.3	1.6	7.014
1.0	1.0	2.739
10.0	0.4	0.423
0.3	0.4	0.438

Table 1: List of a few selected signal samples. The table displays the ALP mass, the coupling strength, and the rounded cross section from MadGraph. For each sample, 10^6 events were produced.

pole run at the FCC-ee. This allows us to directly see the impact of the ALP parameters on the cross section and subsequently on the number of events. As expected, the samples with greater coupling constant, like $m_a = 3GeV$, $c_{\gamma\gamma} = 1.6$ have a higher number of events compared to $m_a = 0.3GeV$, $c_{\gamma\gamma} = 0.4$.
For both gen and reco levels, the plots have the highest number of events for three photons. Although we would expect three generated and reconstructed photons for the signal, there are sometimes additional photons in an event from electromagnetic showers in Pythia. Moreover, the photons are sometimes not detected or the ALP does not decay within the calorimeter, leading to less than three photons in an event.

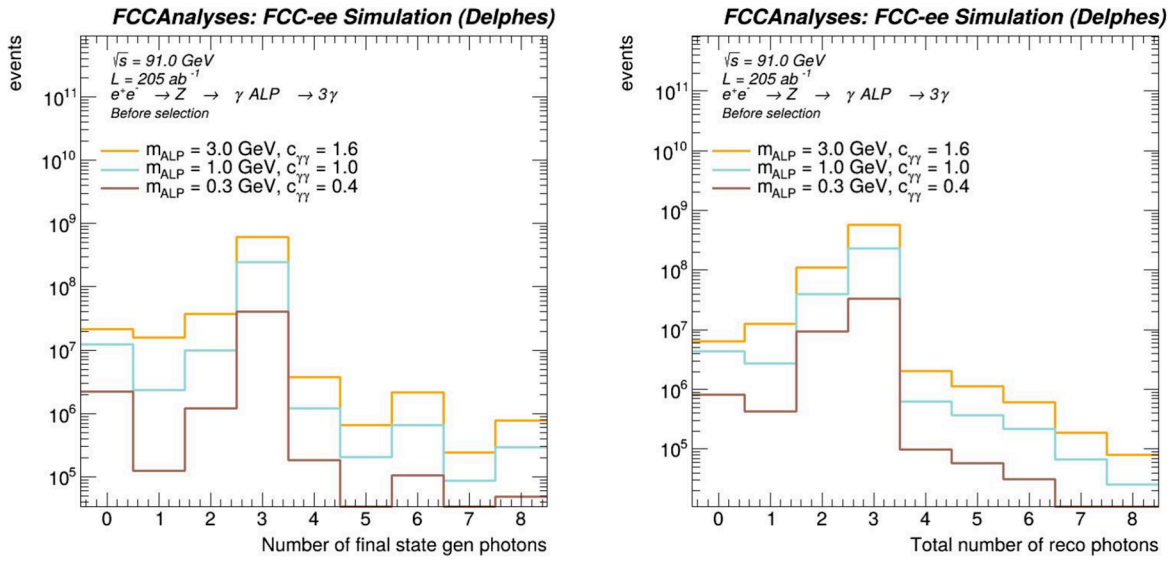

(a) (b)

Figure 8: Number of "gen" level (a) and "reco" level (b) photons per event for three different choices of ALP coupling and mass. Both histograms are scaled to the expected number of events during the Z-pole run at the FCC-ee.

Further interesting variables to look at, for this process, are the angles between the particles. Specifically, the angular separation between the produced final state photons is of interest due to the kinematic nature of the signal process. Although Feynman diagrams

do not, in principle, carry information about relative positions and angles, looking at the diagram for the signal process in Figure 5 still helps to imagine the angular differences between the produced final state photons. The first photon in this process comes from the Z-boson and is produced in conjunction with the ALP. That photon will be referred to as the "leading" photon because it is expected to be the highest momentum photon. The second and third photons, which together will be referred to as the "diphoton", are produced from the ALP decay. The photons in the diphoton system are expected to be collimated, while the diphoton and the leading photon are expected to be back-to-back. To highlight this trait of the process, the variable ΔR between photons is calculated. The definition of the variable is:

$$\Delta R = \sqrt{(\Delta\eta)^2 + (\Delta\phi)^2}. \tag{7}$$

This variable is commonly used in collider experiments and describes the separation between two objects with the pseudorapidity η and azimuthal angle ϕ. The difference of the respective angles of two particles is then written as $\Delta\eta$ and $\Delta\phi$. For an illustration of the angles in the coordinate system of a detector, refer to Figure 4.
The plots of the angles between the reco photons (Figure 9) confirm the expected difference of the angles between the three photons of the signal. For all samples, the ΔR plot displays a strong peak for very low ΔR values, which means that the two photons are close in space and collimated. This corresponds to the photons that decay directly from the ALP. The second peak at around π corresponds to the measurement between the leading photon and the diphoton, which share a bigger angular separation since the leading photon and the diphoton are expected to fly back-to-back after the Z-boson decay.
To examine how the momenta of the signal process is distributed among the photons in each event, the plot in Figure 10 was created. This will be very insightful for later selections, after the momenta of background events is examined. It is noticeable that there is a flat distribution of photon momenta between 2 GeV and 44 GeV and a significant peak at around 45 GeV. This peak comes from the leading photon while the entries for the lower momenta come from the two ALP photons. These two photons can share varying momenta among themselves in each event as long as the total momentum is conserved, which is why the distribution is evenly spread out until 44 GeV.

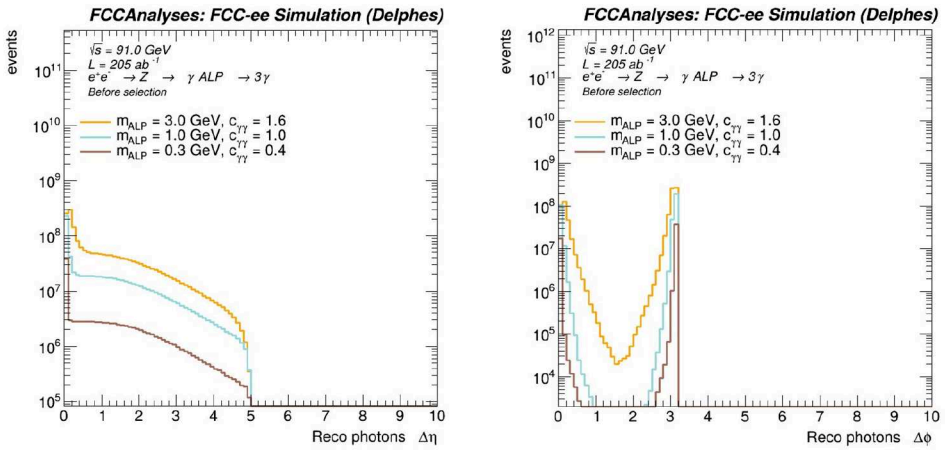

(a) (b)

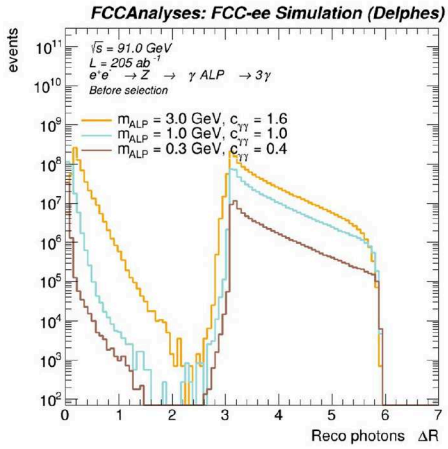

(c)

Figure 9: Difference of the angles $\Delta\eta$ (a), $\Delta\phi$ (b), and ΔR (c) between the reconstructed photons of an event, for three different choices of ALP coupling and mass. The histograms are scaled to the expected number of events during the Z-pole run at the FCC-ee.

Due to the kinematic nature of the process, the leading photon has a momentum of about 45 GeV. This can be shown with a quick calculation using four-vectors:
If we choose the Z-boson as our rest frame, the four-vectors of the boson, the ALP, and the leading photon can be written as

$$p_z = \begin{pmatrix} m_z \\ \vec{0} \end{pmatrix}, p_\gamma = \begin{pmatrix} |\vec{P}_\gamma| \\ \vec{P}_\gamma \end{pmatrix}, p_a = \begin{pmatrix} E_a \\ \vec{P}_a \end{pmatrix},$$

where m_z is the mass of the Z-boson, $\vec{P}_\gamma$ is the momentum of the photon and E_a and $\vec{P}_a$ are the energy and momentum of the ALP respectively. Setting up the equation and solving it for E_γ then looks like this:

$$
\begin{aligned}
p_a^2 = (p_z - p_\gamma)^2 &= m_z^2 + 0 - 2(m_z E_\gamma - \vec{P}_z \vec{P}_\gamma) \\
&\Leftrightarrow m_a^2 = m_z^2 - 2(m_z E_\gamma - 0) \\
&\Leftrightarrow E_\gamma = \frac{m_z^2 - m_a^2}{2m_z} \approx \frac{m_z}{2} \qquad for \quad m_a << m_z \quad .
\end{aligned}
$$

Since a photon does not have a rest mass, E_γ is equal to the photon's total momentum. Since the Z-boson mass is 91 GeV, the momentum of the leading photon is ~45 GeV, explaining the peak in Figure 10. The leading photon's momentum will be further examined in Section 4.3, "Event selections".

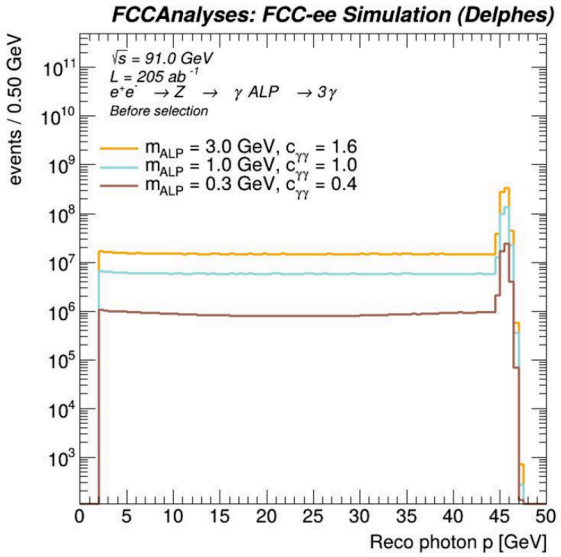

Figure 10: Total momentum of the reconstructed photons, for three different choices of ALP coupling and mass. The histograms are scaled to the expected number of events during the Z-pole run at the FCC-ee.

4.2 Background

For a realistic analysis of a particle collision event, it is necessary to include possible background processes because, in real measurements, we will have to look for the signal among all background events, which might often have higher cross sections. Electron-positron collisions can lead to a variety of processes and some of them may appear similar to the signal that we want to study, making it more difficult to isolate the ALP signal process.

Accordingly, multiple background events have been examined to come closer to realistic conditions for reconstructing the signal. BSM background events will not be considered for this analysis.

Following SM background events have been studied:

Background events

$$Diphoton : e^+e^- \to \gamma\gamma$$
$$Triphoton : e^+e^- \to \gamma\gamma\gamma$$
$$Quadphoton : e^+e^- \to \gamma\gamma\gamma\gamma$$

$$e^+e^- \to e^+e^-$$
$$e^+e^- \to e^+e^-\gamma$$
$$e^+e^- \to e^+e^-\gamma\gamma$$
$$e^+e^- \to e^+e^-\gamma\gamma\gamma$$

The background events have photons in the final state and could potentially imitate the signal event. Especially the triphoton production has a great potential to directly mimic the three final state photons of the signal. In the diphoton production, a single photon might split into an electron-positron pair and then both tracks might be incorrectly reconstructed as separate photons, or an energy mismeasurement could cause a photon to appear as two, giving us three reconstructed photons in total in both cases.
Background events like $e^+e^- \to e^+e^-$ are also included for this analysis since they have very high cross sections (see Table 2) and will very likely experience extra photon radiation in Pythia, which will ultimately lead to photons in the final state.

Background	$e^+e^- \to \gamma\gamma$	$e^+e^- \to \gamma\gamma\gamma$	$e^+e^- \to \gamma\gamma\gamma\gamma$	$e^+e^- \to e^+e^-$	$e^+e^- \to e^+e^-\gamma$	$e^+e^- \to e^+e^-\gamma\gamma$	$e^+e^- \to e^+e^-\gamma\gamma\gamma$
σ[pb]	67.25	2.995	0.06271	4500	118.4	1.993	0.02369

Table 2: Rounded cross sections [pb] from MadGraph for the background events. For each background sample, 10^6 events were produced.

The corresponding Feynman diagrams for a few of the mentioned background processes are illustrated in Figure 11.

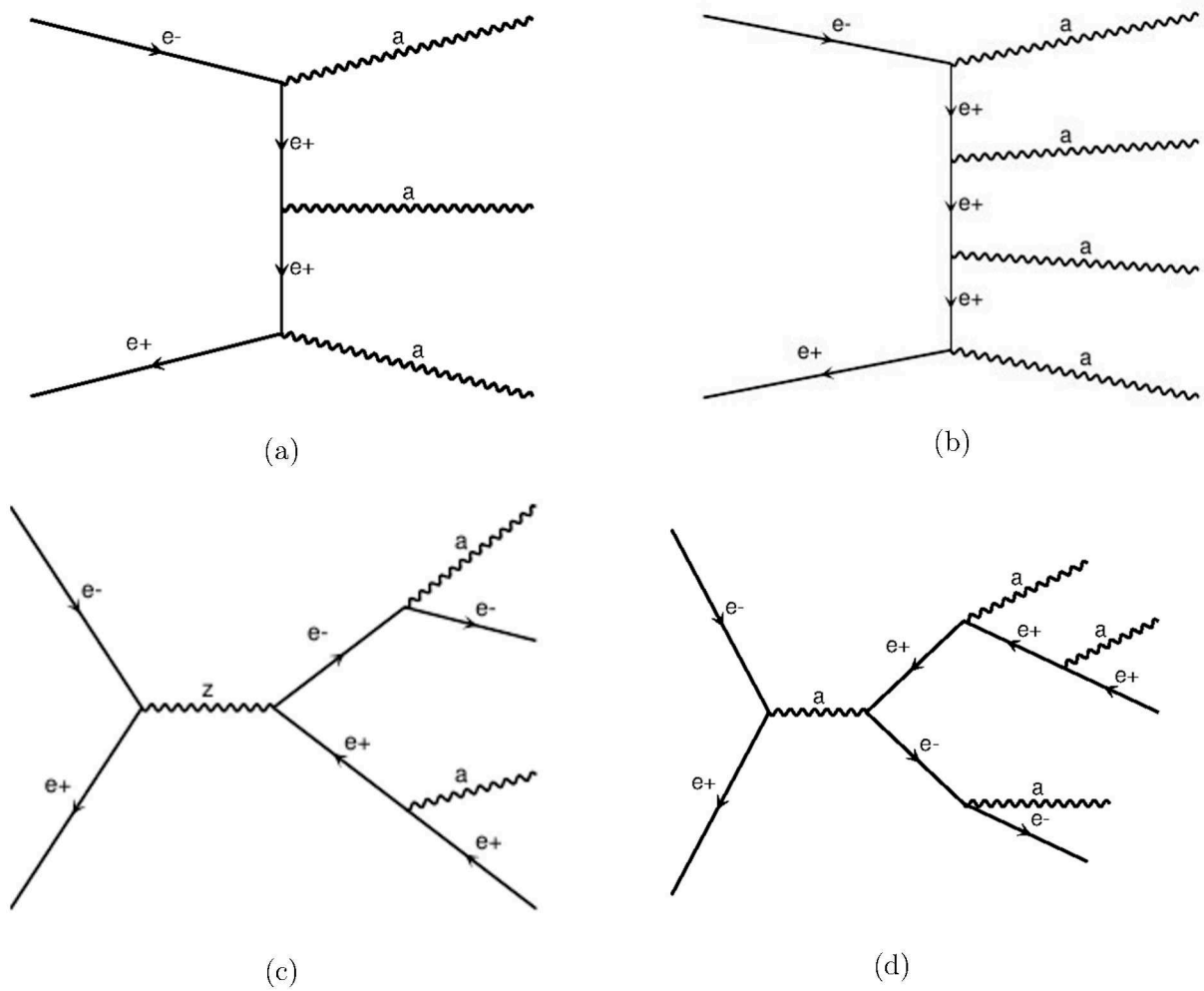

Figure 11: Feynman diagrams of chosen SM background processes produced by MadGraph. Displayed are possible diagrams of the triphoton (a) and quadphoton (b) production, as well as the $e^+e^- \to e^+e^-\gamma\gamma$ (c) and $e^+e^- \to e^+e^-\gamma\gamma\gamma$ (d) production. Here, the letter "a" describes photons and not ALPs.

4.2.1 Technicalities of the background samples production

During the analysis conducted for this thesis, an inconsistency between signal and background events was noticed regarding the parameter constraints coming from MadGraph. When looking at the plots of the transverse momentum of photons at the generation level, a noticeable loss of events at 10 GeV can be seen for the background events (Figure 12(a)). Similarly, a loss of events appears for ΔR at around 0.4 for the background events (Figure 12(b)). This loss of events was not observed for any of the signal events but for all background processes involving photons in the MadGraph generation.
This is due to a setting in the MadGraph *run_card.dat*, which is used to set the parameters of the run. There, the minimum transverse momentum for photons was set to 10 GeV, the minimum ΔR value was set to 0.4, and the maximum $|\eta|$ value to 2.5. For reference, the card settings are shown in Appendix D. These constraints explain the sudden loss of events observed in the p and ΔR distributions of the background events. MadGraph does

not generate these low momentum and close-by photons, meaning that the photons with e.g. less than 10 GeV in momentum in plot (a) have to be generated by Pythia.

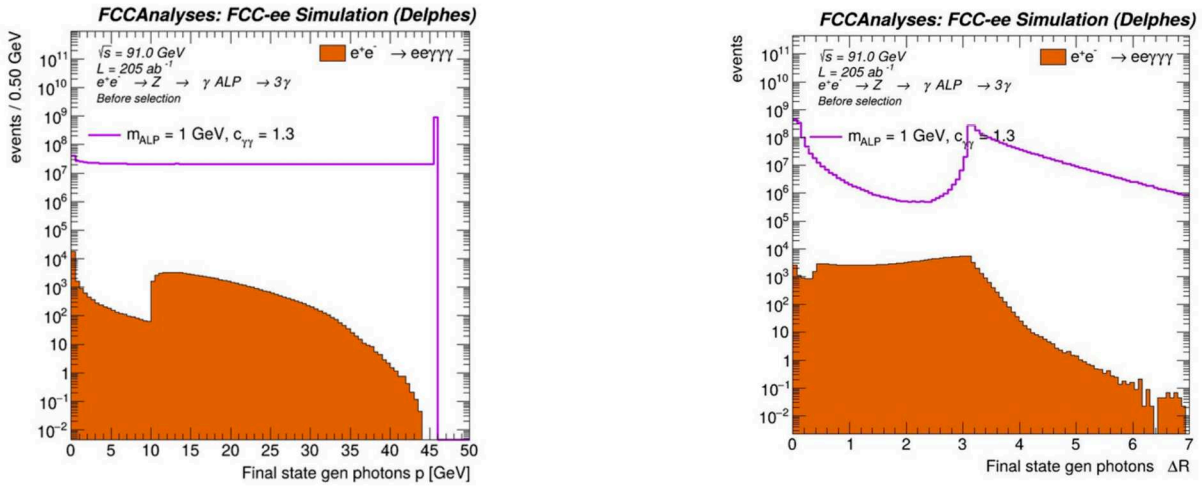

(a) (b)

Figure 12: Illustration of the MadGraph constraints from the *run_card.dat*, which were only applied on the photons from the background events, causing inconsistencies between background and signal photons. The right plot shows the momentum of gen level final state photons (a) and the right plot shows ΔR of the gen level final state photons (b).

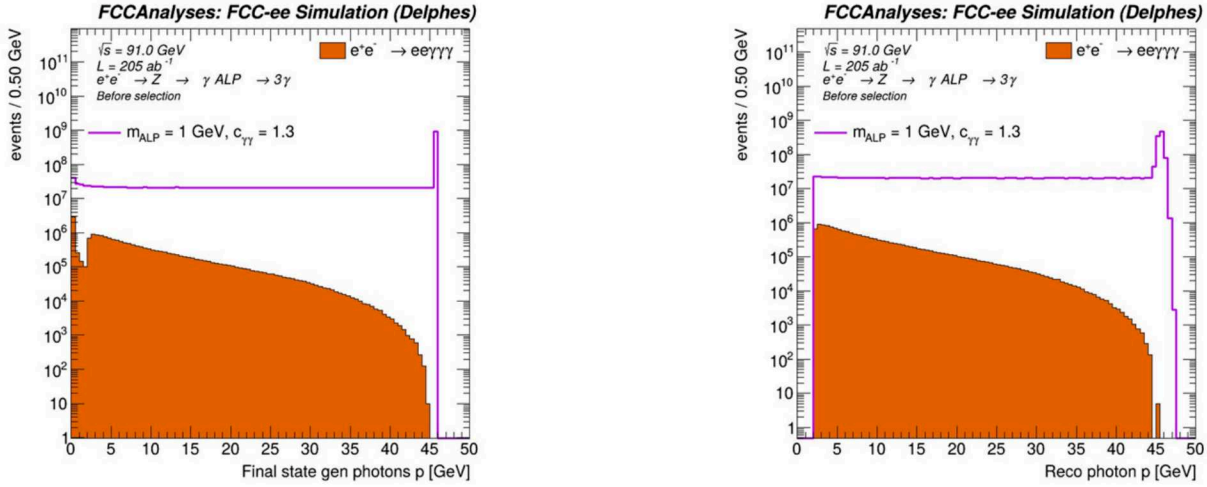

(a) (b)

Figure 13: Plot of the photon momenta with a changed MadGraph parameter constraint for p_T. The loss of events is now shifted to 2 GeV (a) and anyhow does not occur at reco level since tracks can only be reconstructed in the IDEA detector for $p_T > 2$ GeV, leaving us now with a smooth distribution (b).

However, the signal photons are not affected by these constraints, as can be seen in the same plots. Additionally, the signal samples' MadGraph outputs (.lhe files) were checked and many events could be found that had photons with a transverse momentum of less than 10 GeV, verifying that the settings affected only the background events.

To make everything more consistent, the backgrounds were recreated with new settings of the MadGraph *run_card.dat*. The constraint on photon p_T was reduced to $p_T > 2GeV$ (Figure 13(a)). At reco level, the IDEA card prevents reconstruction of photons with less than 2 GeV in p_T anyway, leaving us with a smooth distribution (Figure 13(b)).
Furthermore, the minimum ΔR constraint in the card was lowered to $\Delta R > 0.01$ to allow more collimated photons in the background events, which could mimic our signal.
Finally, the η constraint was kept and is applied as an object selection on all gen and reco level signals and backgrounds due to detector constraints. Figure 14 shows the η distribution of the photons before and after applying the $|\eta|$ object selection on the photons.
For the analysis conducted in this thesis, this object selection has been applied to all events.

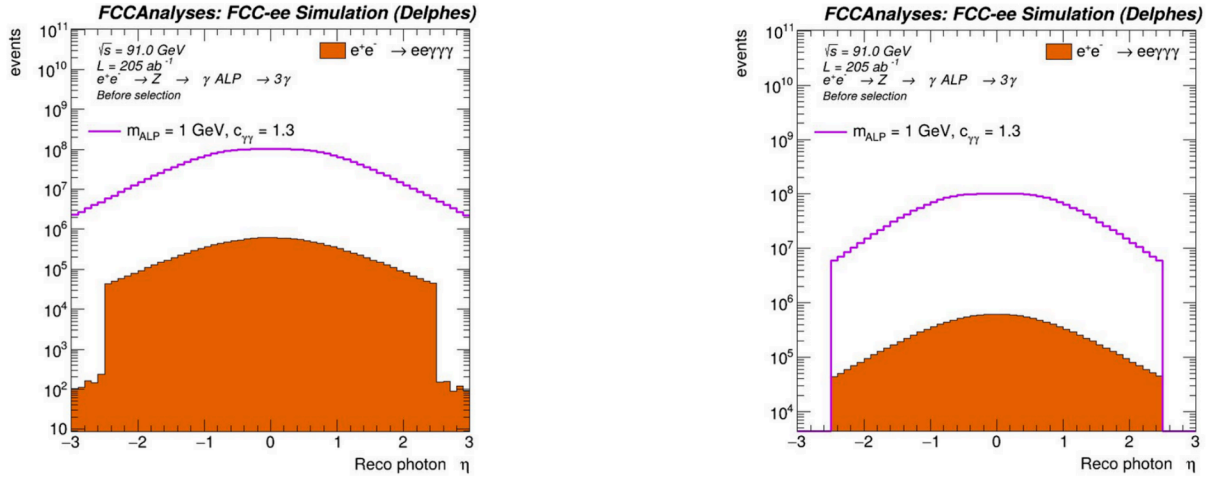

(a) (b)

Figure 14: Illustrating the η distribution of the reconstructed photons before applying any object selections. The background event photons with $|\eta|$ values between 2.5 and 3 are from Pythia because the photons from MadGraph do have a constraint $|\eta| < 2.5$ (a). The right plot shows the distribution after applying an $|\eta|$ object selection for all background and signal events.

4.3 Event selections

To achieve a good sensitivity for the ALP signal detection at the FCC-ee, it is necessary to increase the signal-to-background ratio by applying selection criteria to the collision events that favor the signal. Therefore, the physics behind the events has to be understood to predict which variables would be suitable for selections.
For a detailed examination of the signal and background events, the plots are normalized to unit area, which allows for direct comparison of the histogram shapes, regardless of each sample's cross section.
Firstly, we require zero reconstructed electrons in each event to target the removal of the

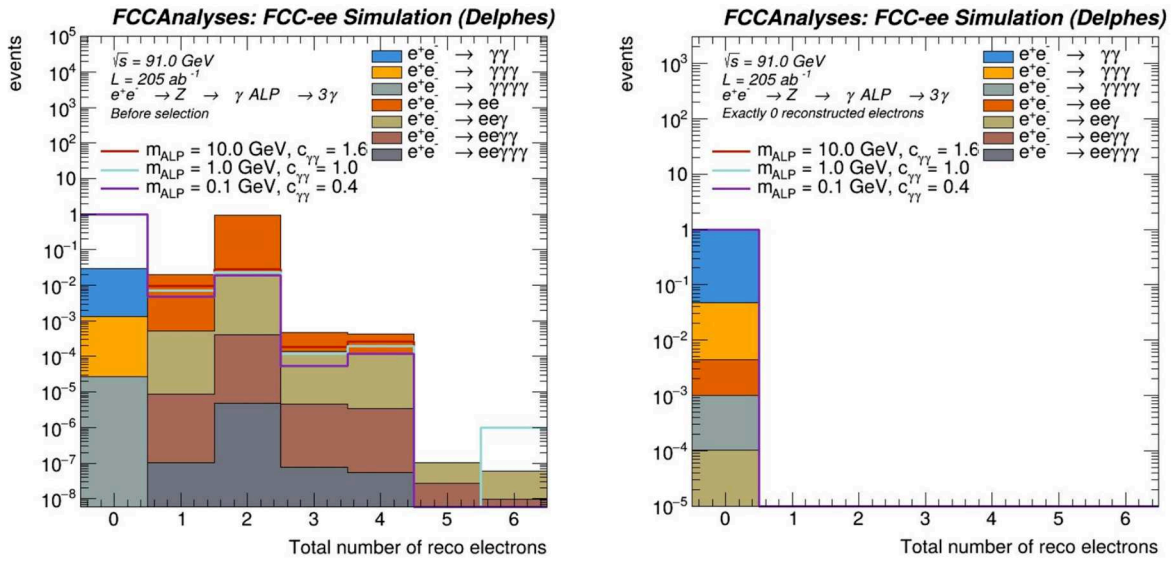

(a) (b)

Figure 15: Number of reconstructed electrons before (a) and after (b) requiring exactly zero reconstructed electrons in an event (Selection 1), for all background processes and three choices of ALP masses and couplings. This is the first event selection made for the analysis. The histograms are normalized to unit area.

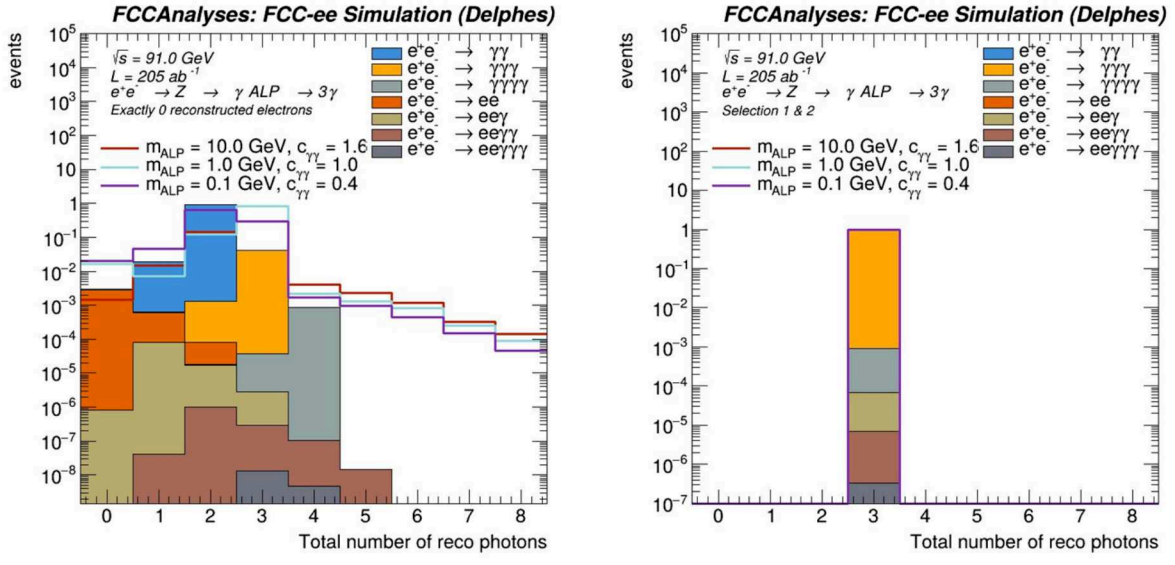

(a) (b)

Figure 16: Number of reconstructed photons before (a) and after (b) requiring exactly three reconstructed photons for each event (Selection 2), for all background processes and three choices of ALP masses and couplings. Selection 1, which requires zero reco electrons, is already applied to both plots. The histograms are normalized to unit area.

high cross section backgrounds with electrons in the final state (see Section 4.2). This keeps almost all of the signal events while removing a large number of background events. The plot in Figure 15 (a) shows that the signal samples peak for 0 reconstructed electrons and that the proposed requirement cuts off a big part of the background with electrons in

the final state. The diphoton, triphoton, and quadphoton background processes are not affected by this selection, as can be seen in the same plot and Table 4.
A second selection criterion requires exactly three reconstructed photons in each event (Selection 2). This is the number of photons expected in each signal event (Equation 4) and would, as can be seen in Figure 16, completely remove the diphoton background events and the remaining $ee \to ee$ background process. A large part of the quadphoton and the remaining $ee \to ee\gamma$ would be removed as well. The $ee \to ee\gamma\gamma$ and $ee \to ee\gamma\gamma\gamma$ processes, which make up a significantly smaller part of the total background, would also be slightly reduced.
In Section 4.1, the ΔR variable was discussed, and its behavior for our signal process was examined. The photons in the diphoton system, which are produced by the boosted ALP, are collimated, while the diphoton and the leading photon are expected to be back-to-back. This kinematic trait of the process can be used to distinguish it from background events. For this, the variable of $\min\Delta R$ is introduced, which computes the minimum angle shared between the reconstructed photons of each event. Ideally, for the signal, we would expect $\min\Delta R$ to be the angle shared between the two photons decaying from the ALP. Indeed, Figure 17 shows that the signal peaks for small $\min\Delta R$ values below 1, which are very likely from the collimated diphoton. It is also noticeable that for bigger ALP masses, the peak shifts towards bigger $\min\Delta R$ values because the ALP is less boosted and the diphoton becomes less collimated as a result. The background, on the other hand, has a flatter distribution in $\min\Delta R$. Hence, a tighter selection would be effective here as well. Accordingly, the third selection made, after analyzing the plot, was to require $\min\ \Delta R < 1$ for the reconstructed photons (Figure 17[(b)).
Lastly, it is worth looking at the distribution of the momenta again. The photon decaying directly from the Z-boson, which is referred to as the leading photon, or in the plots as "$photon_0$", plays a crucial role in identifying the signal event compared to common background events of the process. As was proven in a calculation in Section 4.1, $photon_0$'s momentum is around 45 GeV. The plots validating this calculation are depicted in Figure 18, where it can be seen that the leading photon's momentum at reco level peaks at around 45 GeV. A fourth selection criterion, requiring a minimum momentum threshold for $photon_0$ of 42 GeV (Selection 4) effectively removes much of the quadphoton background events while still keeping the majority of the signal events (Figure 18(b)). The remaining triphoton background overlays almost perfectly with the signal, making it difficult to make more selections.
To further investigate possible selections for this process and to see how well the ALP mass would be reconstructed, a variable for the invariant mass was introduced. Generally, the ALP mass and momentum cannot be measured directly since the particle leaves no tracks in the tracker. Hence, the daughter particles have to be used to reconstruct the ALP's properties. The calculation uses the two reconstructed photons decaying from the ALP ($photon_1$ and $photon_2$) and calculates the invariant mass of their united four-vector,

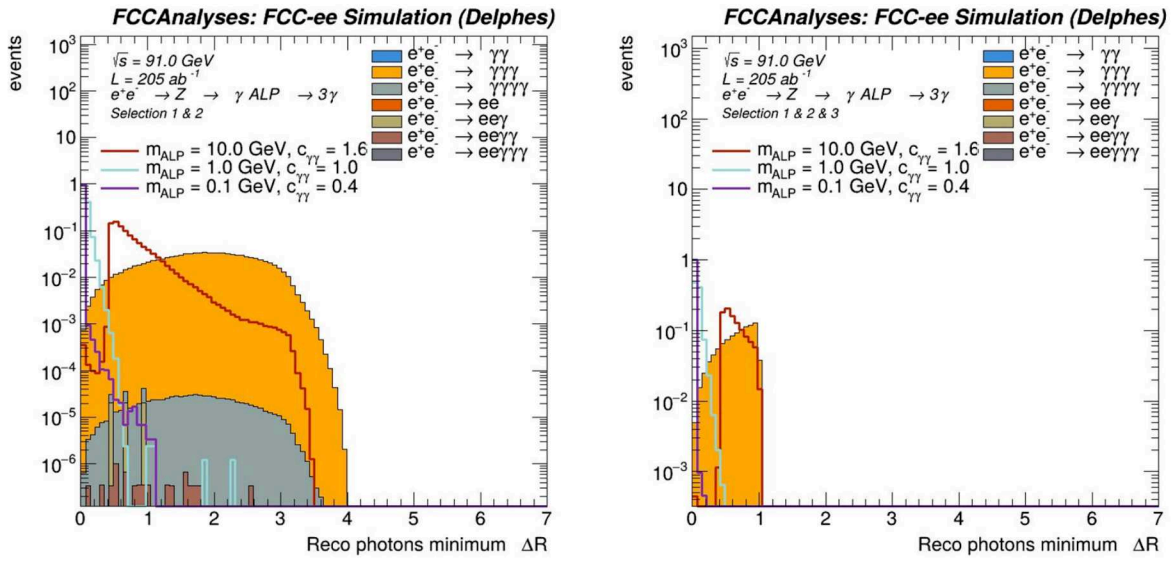

(a) (b)

Figure 17: The min ΔR of reco photons before (a) and after (b) requiring $\Delta R < 1$ (Selection 3), for all background processes and three choices of ALP masses and couplings. Selections 1 and 2 are already applied to both plots. The histograms are normalized to unit area.

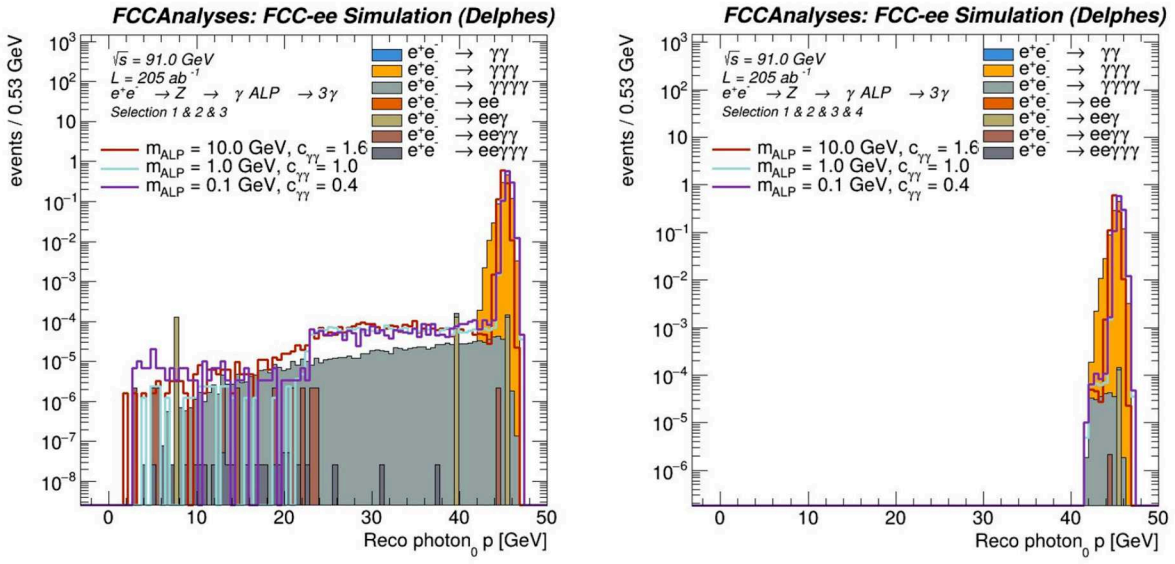

(a) (b)

Figure 18: Momentum of the leading photon ($photon_0$) before (a) and after (b) requiring $p > 42GeV$ for the reco $photon_0$'s momentum (Selection 4), for all background processes and three choices of ALP masses and couplings. Selections 1, 2, and 3 are already applied to both plots. The histograms are normalized to unit area.

which should equal the mass of the ALP. Two different ways of determining $photon_1$ and $photon_2$ were explored. The first method (method 1) chooses the second and third leading photon in the event, essentially picking the photons with the second and third highest momentum (Figure 19(a)). This aims to target the photons decaying from the ALP, while

the photon decaying from the Z-boson has the highest photon momentum of the system, as was explained earlier in Section 4.1. The second method (method 2) picks the pair of photons with the smallest angular separation ("minΔR"), which are also expected to be the two photons from the ALP decay (Figure 19(b)). For this, a new function, which collects the photon indices of the two photons that share the smallest angular separation, had to be defined in the source files. With that new collection of photons, the invariant mass can be calculated in the same way. A comparison of these two methods after applying all four selections is shown in Figure 19. Figure 20 depicts the actual ALP mass at "gen" level.

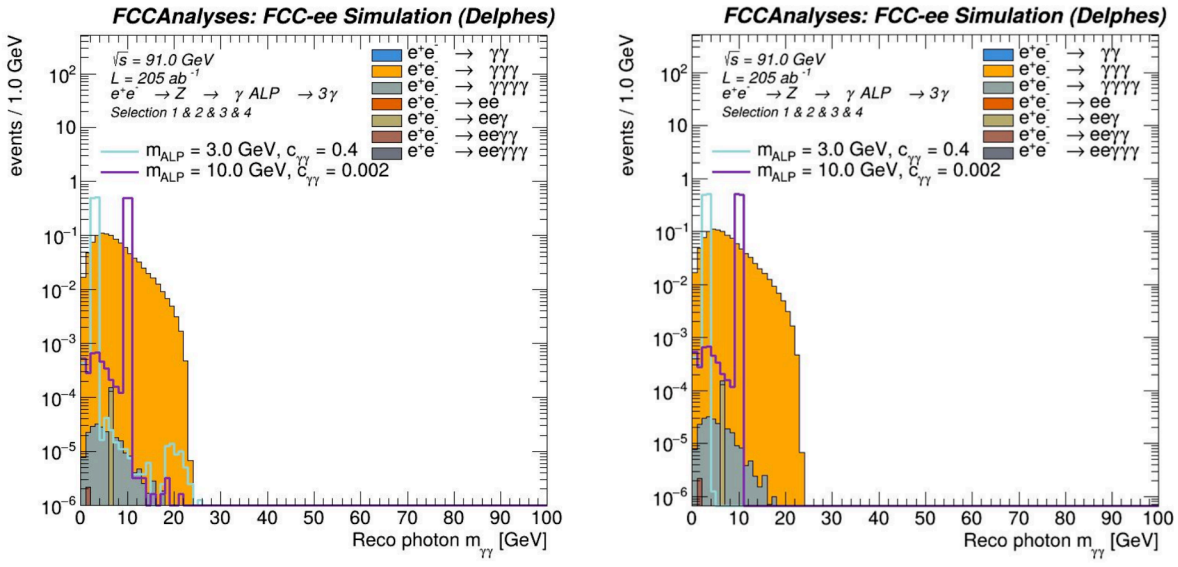

(a) (b)

Figure 19: Reconstructed invariant mass of the two photons decaying from the ALP with method 1 (a) and method 2 (b), for all background processes and two choices of ALP masses and couplings. The histograms are normalized to unit area.

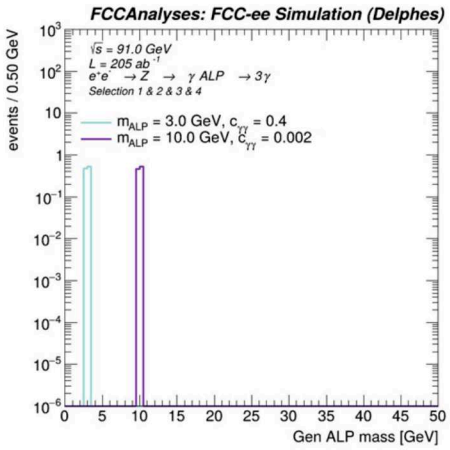

(a)

Figure 20: ALP mass at gen level, for two choices of ALP masses and couplings. The histograms are normalized to unit area.

As can be seen, both methods deliver very similar results for the reconstructed ALP mass. The different samples peak correctly for the invariant mass values that correspond to the respective ALP mass of the sample. The fact that both methods (choosing the photons with the second and third highest momentum/choosing the photons that share the minΔR angle) give us almost identical plots proves that the previous selections made were effective in ensuring that the two reco photons with the smallest angular separation and second and third highest momentum are indeed the diphoton from the ALP (for signal events).
Sometimes, smaller ALP masses are reconstructed because the wrong photons might be selected. Photons from Pythia radiation might at times have the smallest angular separation or, if the ALP decays outside of the detector, photons from Pythia can be chosen for the second and third highest momentum of the system.
The background in the plots is spread out and it is not possible to make further selections here since, for example, signal samples with higher ALP masses would be even further to the right side of the plots. If a specific ALP mass is envisioned for future searches, the selections can be optimized with this variable of the invariant mass to obtain better separation of signal and background events.
Furthermore, the two mentioned methods were used to determine the reconstructed momentum of the ALP by calculating the total momentum of the diphoton. Figure 21 (a) shows the result using method 2 and a comparison to the gen level ALP momentum in Figure 21 (b). Here, again, no effective selections can be made.
Lastly, another new variable was introduced to attain the angular separation ΔR between the leading photon and the diphoton, which are expected to fly back-to-back. For this, a new function in the source script was introduced, which first calculates the united four-vector of the diphoton system and then its angle to the leading photon. The results are

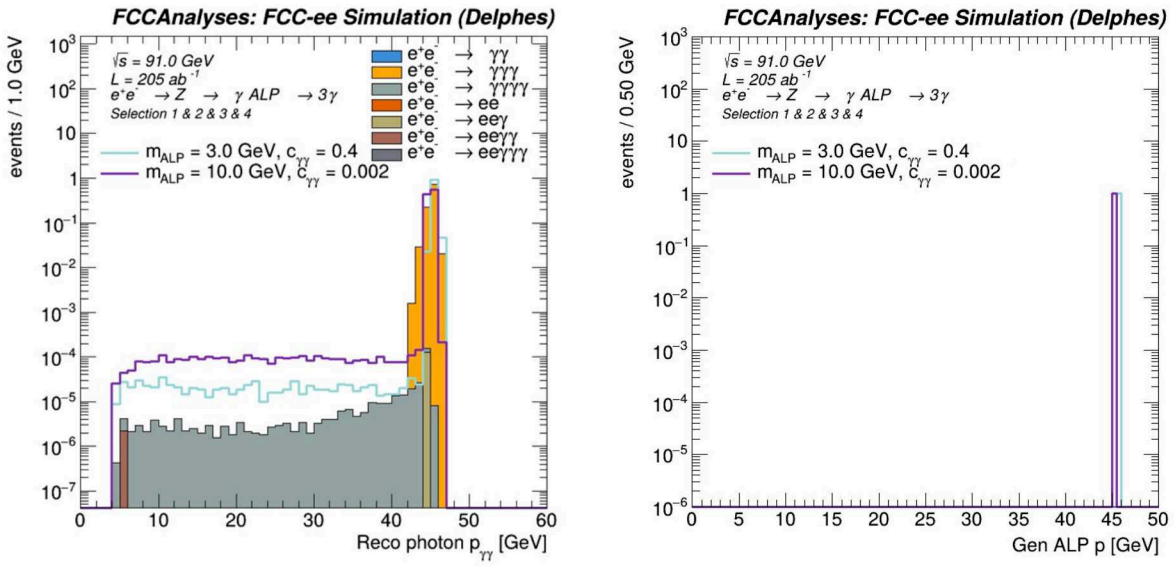

(a) (b)

Figure 21: Reconstructed total momentum of the two photons decaying from the ALP with method 2 (a), for all background processes and three choices of ALP masses and couplings. For comparison, the ALP momentum at gen level is shown in (b). The histograms are normalized to unit area.

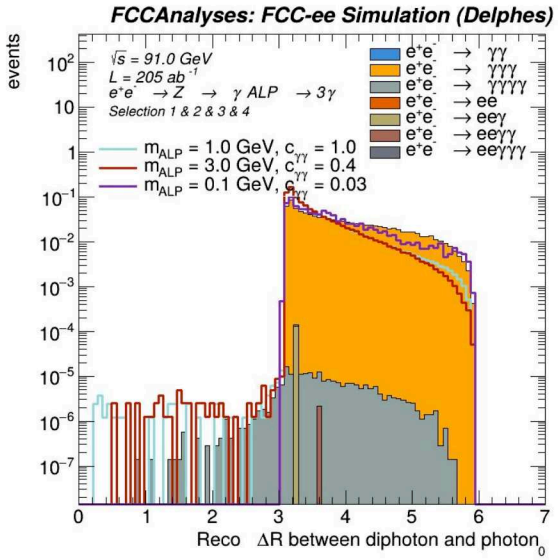

Figure 22: ΔR between the leading photon and the diphoton at reco level, for all background processes and three choices of ALP masses and couplings. The histogram is normalized to unit area.

plotted in Figure 22 and, as expected, the signal is peaking at around π. However, the background behaves almost identically to the signal, leaving us no room to make further selections. A summary of the final event selection requirements, that were used for this analysis, is shown in Table 3.

A cut flow table that sums up the final four selections applied for this analysis is displayed

		Selection Criteria
Selection 1	**Vetoes**	No reconstructed electrons
Selection 2	**Final State**	Exactly 3 reconstructed photons
Selection 3	**Angles**	$\min \Delta R < 1$
Selection 4	**Momentum**	$p > 42$ GeV for leading photon ($photon_0$)

Table 3: Summary of the event selections.

in Table 4. The selections are cumulatively added to each other to understand what happens to the number of expected events for the Z-pole run at the FCC-ee after each step. Each selection step includes all prior selections and the expected number of events N_{exp} that remain at each stage of the selection is calculated using Equation 6. Additionally, the percentage of the initial event number (prior to any selections) is calculated. The table shows that the selections were effective in removing a large number of background events, except for the triphoton process, where 15% of the original number of expected events remain after all selection criteria are applied. The majority of the signal events displayed in the table are maintained after the selections. The table in Appendix A shows an overview of all signal samples that were produced for this thesis.

		All events		0 electrons		+ 3 photons		+ min$\Delta R < 1$		+leading photon p > 42 GeV	
Signal events		N_{exp}	%	N_{exp}	%	N_{exp}	%	N_{exp}	%	N_{exp}	%
m_a[GeV]	$c_{\gamma\gamma}$										
1	1	2.75e+08	100	2.67e+08	97	2.26e+08	82	2.26e+08	82	2.26e+08	82
3	0.4	4.39e+07	100	4.24e+07	97	3.56e+07	81	3.55e+07	81	3.54e+07	81
0.1	0.4	4.40e+07	100	4.30e+07	98	1.30e+07	30	1.30e+07	30	1.29e+07	29
10	1.6	6.79e+08	100	6.54e+08	96	5.47e+08	80	4.26e+08	63	4.25e+08	63
10	0.002	1.06e+03	100	1.02e+03	96	8.54e+02	81	6.66e+02	63	6.65e+02	63
Background events		N_{exp}	%	N_{exp}	%	N_{exp}	%	N_{exp}	%	N_{exp}	%
$e^+e^- \to \gamma\gamma$		1.38e+10	100	1.38e+10	100	0.	0	0.	0	0.	0
$e^+e^- \to \gamma\gamma\gamma$		6.14e+08	100	6.14e+08	100	5.96e+08	97	9.16e+07	15	9.16e+07	15
$e^+e^- \to \gamma\gamma\gamma\gamma$		1.29e+07	100	1.29e+07	100	5.05e+05	3.9	9.58e+04	0.75	2.16e+04	0.17
$e^+e^- \to e^+e^-$		4.52e+11	100	4.97e+07	0.011	0.	0	0.	0	0.	0
$e^+e^- \to e^+e^-\gamma$		1.19e+10	100	1.47e+06	0.012	3.57e+04	0.0003	3.57e+04	0.0003	1.19e+04	0.0001
$e^+e^- \to e^+e^-\gamma\gamma$		2.00e+08	100	2.10e+04	0.011	4.00e+03	0.003	2.20e+03	0.0011	2.00e+02	0.0001
$e^+e^- \to e^+e^-\gamma\gamma\gamma$		2.38e+06	100	2.83e+02	0.012	1.95e+02	0.0082	7.14e+01	0.003	0.	0

Table 4: Cut flow table of the sequential application of the four event selections, where each selection step is cumulative. The table displays the ALP mass and coupling strength of selected signal samples and all background events. N_{exp} is the expected number of events that remain at each stage of the applied selection for the Z-pole run at the FCC-ee and is calculated using Equation 6. The % columns show what percentage of the initial number of events (prior to any selections) remain after the specified selections.

4.4 Timing variable

The ALP signal event discussed in this thesis has a very special trait, which makes it stand out from other background processes: a displaced vertex. For long-lived ALPs, the diphoton is produced at a vertex, significantly displaced from the interaction point (IP) of the collision. This particular characteristic could be taken advantage of for further event selections.

Because neither the ALP nor the photons leave tracks in the tracker, the displaced vertex position cannot be directly measured by the detector. This also means that the ALP's decay length and lifetime cannot be directly accessed at reco level. Figure 23 shows what the decay length of the ALP looks like at gen level. It can be seen that for smaller coupling strengths, the ALP's lifetime becomes longer, which is in agreement with Equation 3.

To make use of the displaced vertex coming from the ALP, calorimeter and precision timing variables are needed, which are yet to be implemented in the FCCAnalyses framework. Nevertheless, this Section will elaborate on the attempt to artificially retrieve timing variables.

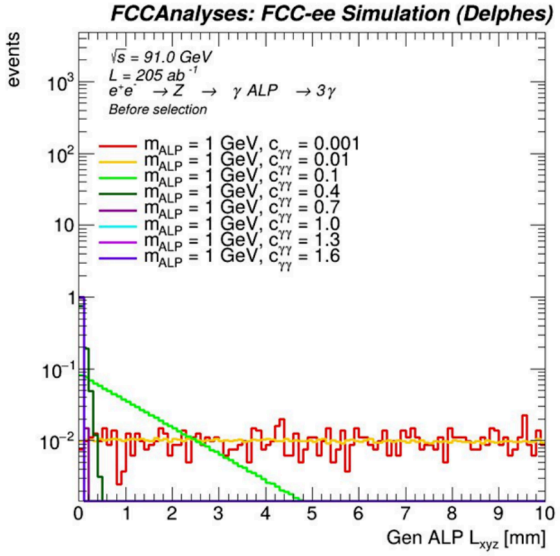

Figure 23: ALP decay length L_{xyz} at gen level.

The motivation for obtaining timing variables builds upon the foundation that the background process and $photon_0$ from the signal process are prompt, meaning that the photons point back directly to the IP, whereas for the signal, the diphoton should be detected with a slight time delay due to the displaced vertex. Figure 24 illustrates this through simple geometry, where it is shown that the length of the non-prompt (IP to ALP decay vertex to calorimeter) trajectory is longer than the prompt one (IP to calorimeter).

To get the trajectory lengths, a new function, which calculates the coordinates of the calorimeter hit of a prompt photon, was introduced in the source file. This needs to be done since the CalorimeterHit.position variable from the TTree does not tell us whether

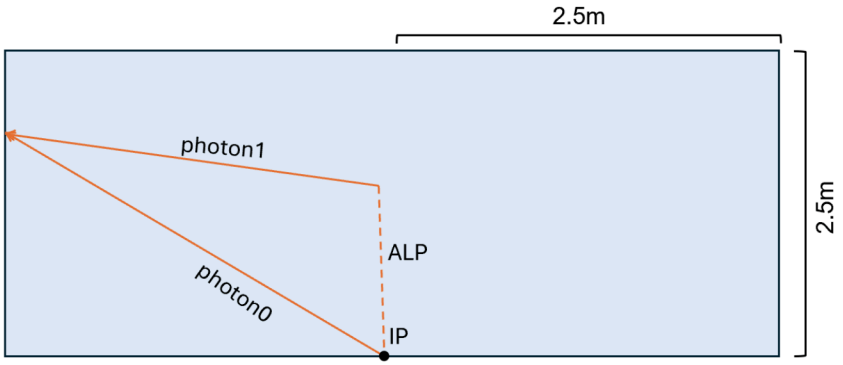

Figure 24: Simplified illustration for the comparison of the lengths of the prompt ($photon_0$) and non-prompt (ALP+$photon_1$) trajectories. This is not a literal decay possibility, since it would not conserve the total momentum. Instead, this illustration shows that, according to basic geometry, the non-prompt trajectory length is longer than the prompt one. The inner radius of the IDEA calorimeter is 2.5 m.

a hit is coming from a prompt or non-prompt photon. It is important to distinguish whether a calorimeter hit is coming from $photon_0$ (leading photon, which is assumed to be prompt and to be coming directly from the IP) or from the diphoton (not prompt, displaced) in order to calculate the correct length of the trajectory.
Firstly, the function uses $photon_0$'s momentum to find the coordinates of when the inner part of the calorimeter would be hit. Here, the geometry of the IDEA detector (Figure 3) was employed for the calculation.
Secondly, to calculate the length of the path traveled by the ALP + displaced photon, one of the diphoton's momentum is used as well as the ALP production vertex coordinates from gen level to calculate the coordinate of the calorimeter hit.
With these length measurements, it is possible to calculate travel times and to plot Δt, which would be the travel time difference of $photon_0$ and ALP+$photon_1$ (or $photon_2$). For background events, this should be zero, whereas for the signal, a non-zero Δt value is expected. We assume that ALPs travel at the speed of light in this analysis. To prove this assumption is valid, the variable $\beta = \frac{v}{c} = \frac{P}{E}$ was calculated at gen and reco level using the ALP's momentum and energy. Figure 25 shows the results of that and it can be seen that the approximation is reasonable, for the ALP masses and couplings probed in this analysis. For much heavier ALP masses than the shown samples, $\beta \neq 1$ might have to be incorporated in the travel time calculation for a more detailed analysis.
It should also be mentioned that, depending on the scenario, different Δt values will be obtained. If we only focus on ALPs that decay before reaching the calorimeter, there are four possible decay scenarios to consider (see Figure 26). Ideally, we would get the biggest time difference for a large ALP mass ($\rightarrow$ less collimated) combined with a small coupling ($\rightarrow$ displaced vertex), which is scenario 1) in the graphic. However, this would also mean a low cross section for the signal, as was discussed in Section 4.1.
A detailed analysis of the timing variables is beyond the scope of this thesis. Nevertheless,

a foundation for such an analysis has been established, providing a basis to work on for future projects.

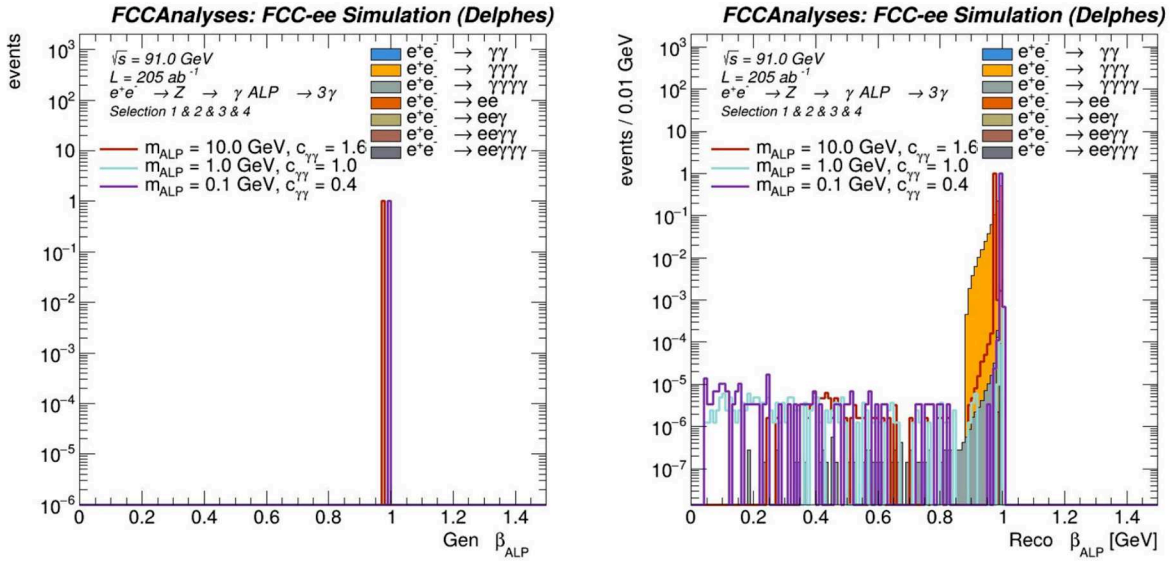

(a) (b)

Figure 25: $\beta = \frac{v}{c} = \frac{P}{E}$ of the ALP at gen (a) and reco (b) level.

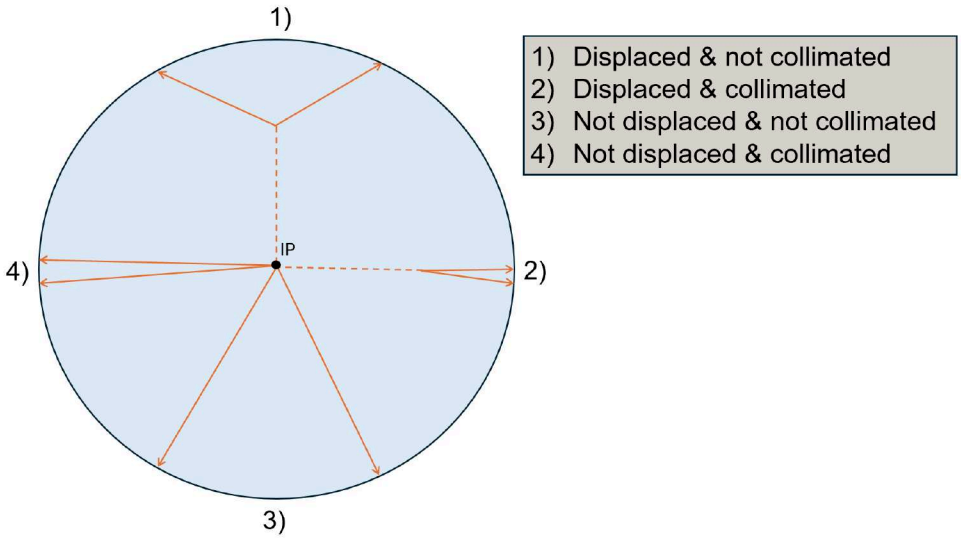

Figure 26: Four different scenarios for an ALP decaying before it reaches the calorimeter, depending on the ALP's mass and coupling. The dashed line represents the ALP and the straight lines represent photons.

5 Results

In the scope of this thesis, many signal points with 10^6 events each were generated. The samples span over ALP masses in the MeV and GeV range as well as over a wide range of coupling constants $c_{\gamma\gamma}$ to explore the discovery reach for ALPs in the FCC-ee. After the aforementioned selections from Section 4.3, the sensitivity was analyzed.
To determine what parameter space the FCC could cover during the Z-pole run, the sensitivity for the detection of the signal process is calculated using

$$s = \frac{n_S}{\sqrt{n_S + n_B}}, \tag{8}$$

[20] where n_S (n_B) is the number of expected events for the signal (background) during the Z-pole run after all selections are applied. This value, s, estimates the signal significance as the size of the signal relative to one standard deviation and it essentially tells us how well a signal can be distinguished from background events.

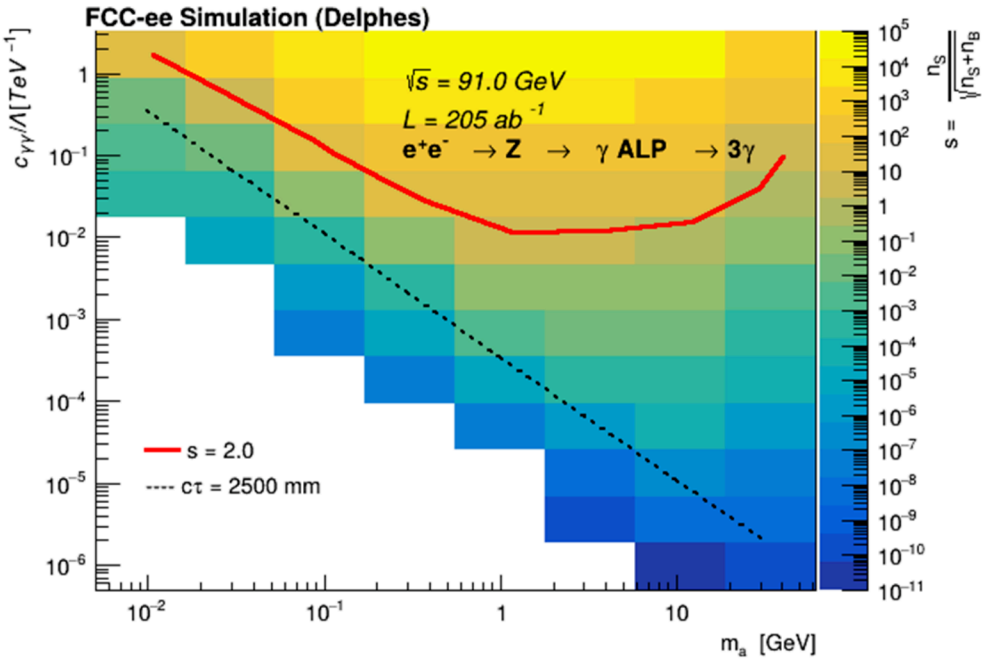

Figure 27: Projected sensitivity of the FCC-ee Z-pole run to the signal process without considering systematic uncertainties. The signal points encompass, on the x-axis, masses ranging from 0.01 GeV to 30 GeV and, on the y-axis, coupling constants ranging from 10^{-6} to 1.6. The z-axis is color-coded and represents low sensitivity values with blue colors and high sensitivity areas with yellow colors. The 2σ ($\sim$ 95% confidence level limit) signal significance is plotted (red line), as well as a dashed line showing $c\tau = 2500mm$.

The sensitivity is calculated for all produced samples in this analysis (see Table in Appendix A for a full list of signal samples) and the final results are plotted in Figure 27. The graph shows the projected results for the sensitivity of the FCC-ee Z-pole run to the ALP detection. The ALP masses and couplings are plotted on a logarithmic scale to cover a

wide range of parameter space. The third dimension of the plot, visualized by color-coded rectangles, shows the sensitivity. Yellow rectangles indicate high-sensitivity areas of the FCC-ee within the ALP parameter space, while blue areas indicate low sensitivity, where detection of the signal is more challenging.

As can be seen from the plot, the sensitivity for the signal detection decreases for lower couplings. This is expected because the cross section also decreases for lower couplings, as discussed in Section 4.1, ultimately leading to a smaller number of expected signal events. The black dashed line in the plot illustrates which combination of ALP mass and coupling strength results in a proper decay length of 2500 mm for the particle. This distance corresponds to the inner part of the calorimeter, based on the geometry of IDEA. Signal samples below this line have a longer lifetime and with that, a longer decay length. Since for this analysis, the applied selections are aiming for ALPs decaying before the electromagnetic calorimeter, the sensitivity is significantly reduced for very long-lived ALPs that decay later. That explains the low sensitivity in the parameter space around and beneath the dashed line.

The white space in the bottom left corner of the plot represents regions where the ALPs are too long-lived and escape the detector volume. During the analysis, it was noticed that Pythia sets the lifetime to zero for these very long-lived ALPs. There was no time to explore this behavior further, but anyhow, we would expect very low sensitivities for this region. These samples are therefore not analyzed.

Furthermore, a line with a sensitivity of s=2 is drawn on the graph to visualize the exclusion limit for a signal significance of 2σ ($\sim 95\%$ confidence level limit).

Lastly, the results from this analysis are compared with existing bounds from other collider experiments searching for ALPs. As Figure 28 shows, the FCC-ee will allow us to significantly extend the ALP search range. The plot demonstrates how much uncovered phase space one could access with the proposed future collider and this analysis strategy. If no significant ALP signal is observed for the FCC-ee, the ALP parameters can be excluded in the corresponding coupling and mass range shown in Figure 28.

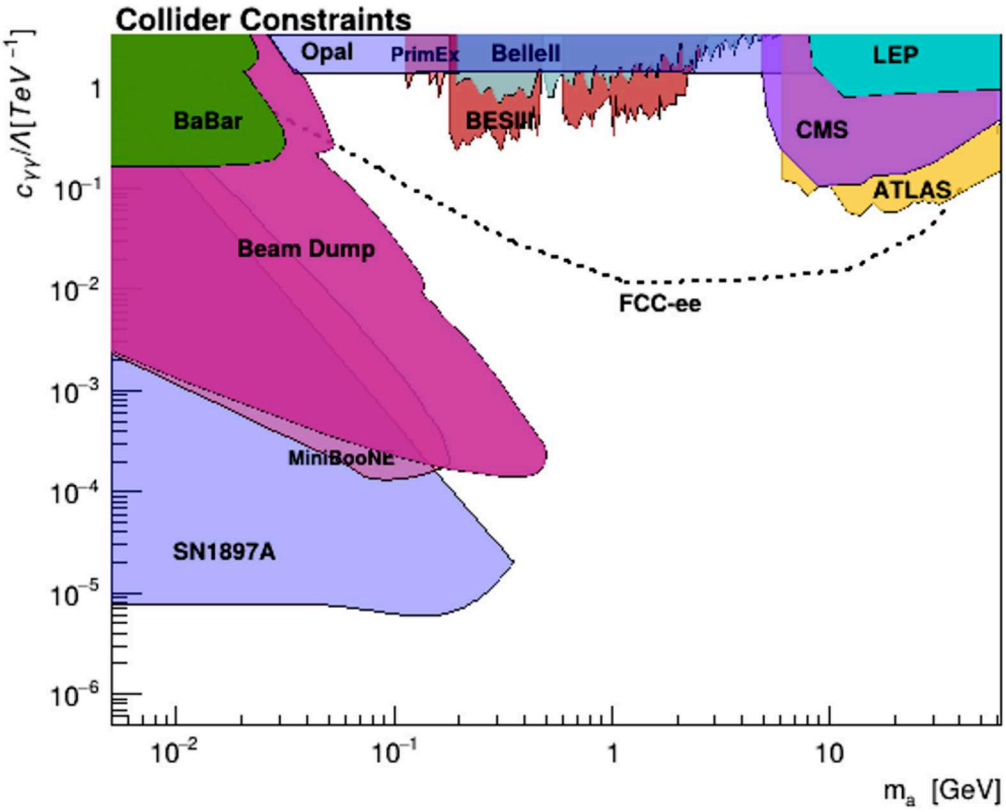

Figure 28: Projected sensitivity of the FCC-ee ($e^+e^- \to Z \to a\gamma \to \gamma\gamma\gamma$) at 95% confidence level limit (black dashed line) in the ALP-photon coupling versus ALP mass plane. Constraints from other collider searches on the ALP parameter space are plotted for direct comparison of the collider's reach. Existing bounds (colored areas) are taken from [28].

6 Conclusion and outlook

This thesis built on previous work on ALPs with the FCCAnalyses framework, and it investigated the FCC's sensitivity to an ALP detection during the Z-pole run. Various ALP masses and coupling constants were analyzed to cover a broad landscape of parameter space. Interesting new discriminating variables were introduced in the source code and analysis scripts to further investigate the physical behavior of the signal process. Accordingly, selections were made to effectively reduce the number of background events while maintaining as many signal events as possible. By increasing the signal-to-background ratio, the sensitivity for an ALP detection was increased and plotted. The analysis resulted in new constraints for ALPs produced in the $e^+e^- \to Z \to a\gamma \to \gamma\gamma\gamma$ signal process, which can be explored at the FCC-ee.

The results indicate that with the FCC-ee and this analysis strategy, the ALP search range can be significantly extended, allowing to probe yet uncovered parts of the ALP phase space (see Figure 28).

There are many possible ways to further extend this work in the future by, for example, utilizing calorimeter timing variables at reco level for event selections, as was elaborated in Section 4.4. Additionally, statistical and systematic uncertainties in the background

and signal efficiency should be included, which was not in the scope of this thesis due to limited time. Another way to generally extend this work is by exploring more possible background events, possibly even BSM background processes.
For now, the FCC remains a proposed next-generation collider, but its future is steadily taking shape through research conducted by physicists around the globe. In the coming years, between 2027 and 2028, CERN member states and international partners will make the final decision on the construction of the FCC [2].

References

[1] Neubert Bauer Heiles. "Axion-like particles at future colliders". In: *Eur. Phys. J. C* 2019.79, 74 (2023). DOI: 10.1140/epjc/s10052-019-6587-9. URL: https://doi.org/10.1140/epjc/s10052-019-6587-9.

[2] *Future Circular Collider*. URL: https://home.cern/science/accelerators/future-circular-collider.

[3] G. Bernardi et al. *The Future Circular Collider: a Summary for the US 2021 Snowmass Process*. 2022. arXiv: 2203.06520 [hep-ex]. URL: https://arxiv.org/abs/2203.06520.

[4] *Host states gear up to work on FCC*. URL: https://fccis.web.cern.ch/host-states-gear-work-fcc.

[5] *FCC:Machine parameters*. Oct. 2024. URL: https://fcc-ped.web.cern.ch/content/machine-parameters.

[6] *FCCeePhysicsPerformance*. URL: https://hep-fcc.github.io/FCCeePhysicsPerformance/#lois-submitted-to-snowmass.

[7] Patrick Janot and Christophe Grojean. *FCC: The physics case*. Mar. 2024. URL: https://cerncourier.com/a/fcc-the-physics-case/.

[8] Franco Bedeschi. "A detector concept proposal for a circular e+e- collider". In: *Proceedings of 40th International Conference on High Energy physics — PoS(ICHEP2020)*. Vol. 390. 2021, p. 819. DOI: 10.22323/1.390.0819.

[9] Juska Pekkanen. "ALLEGRO FCC-ee detector concept & Noble liquid calorimetry". In: *Nucl. Instrum. Methods Phys. Res., A* 1069 (2024), p. 169921. DOI: 10.1016/j.nima.2024.169921. URL: https://cds.cern.ch/record/2917062.

[10] A. Abada, M. Abbrescia, S. S. AbdusSalam, et al. "FCC-ee: The Lepton Collider". In: *European Physical Journal Special Topics* 228 (2019), pp. 261–623. DOI: 10.1140/epjst/e2019-900045-4. URL: https://doi.org/10.1140/epjst/e2019-900045-4.

[11] Izaak Neutelings. *Izaak neutelings*. Accessed: 25-02-2025. URL: https://tikz.net/axis3d_cms/.

[12] Martin Bauer, Matthias Neubert, and Andrea Thamm. "Collider probes of axion-like particles". In: *Journal of High Energy Physics* 2017.12 (Dec. 2017). ISSN: 1029-8479. DOI: 10.1007/jhep12(2017)044. URL: http://dx.doi.org/10.1007/JHEP12(2017)044.

[13] Jaan Einasto. *Dark Matter*. 2010. arXiv: 0901.0632 [astro-ph.CO]. URL: https://arxiv.org/abs/0901.0632.

[14] Vera C. Rubin and W. Kent Ford Jr. "Rotation of the Andromeda Nebula from a Spectroscopic Survey of Emission Regions". In: *apj* 159 (Feb. 1970). DOI: 10.1086/150317.

[15] *Cronin and Fitch detect a difference between matter and antimatter*. URL: https://timeline.web.cern.ch/cronin-and-fitch-detect-difference-between-matter-and-antimatter.

[16] Roberto D. Peccei. "The Strong CP Problem and Axions". In: *Axions*. Springer Berlin Heidelberg, 2008, pp. 3–17. ISBN: 9783540735182. DOI: 10.1007/978-3-540-73518-2_1. URL: http://dx.doi.org/10.1007/978-3-540-73518-2_1.

[17] Fernando Arias-Aragón, Jérémie Quevillon, and Christopher Smith. "Axion-like ALPs". In: *Journal of High Energy Physics* 2023.3 (Mar. 2023). ISSN: 1029-8479. DOI: 10.1007/jhep03(2023)134. URL: http://dx.doi.org/10.1007/JHEP03(2023)134.

[18] Martin Bauer et al. "Axion-like particles at future colliders". In: *The European Physical Journal C* 79.1 (Jan. 2019). ISSN: 1434-6052. DOI: 10.1140/epjc/s10052-019-6587-9. URL: http://dx.doi.org/10.1140/epjc/s10052-019-6587-9.

[19] C. B. Verhaaren et al. "Searches for long-lived particles at the future FCC-ee". In: *Frontiers in Physics* 10 (Sept. 2022). ISSN: 2296-424X. DOI: 10.3389/fphy.2022.967881. URL: http://dx.doi.org/10.3389/fphy.2022.967881.

[20] Lovisa Rygaard. "Long-Lived Heavy Neutral Leptons at the FCC-ee". MA thesis. Uppsala University, High Energy Physics, 2022, p. 48. URL: https://urn.kb.se/resolve?urn=urn:nbn:se:uu:diva-479595.

[21] J. Alwall et al. "The automated computation of tree-level and next-to-leading order differential cross sections, and their matching to parton shower simulations". In: *JHEP* 07 (2014), p. 079. DOI: 10.1007/JHEP07(2014)079. arXiv: 1405.0301 [hep-ph].

[22] Gogolin M., J. Alimena, and L. Rygaard. *Simulating and Investigating Long-Lived Axion-Like Particles at the Proposed FCC-ee*. 2024.

[23] Torbjörn Sjöstrand et al. "An introduction to PYTHIA 8.2". In: *Comput. Phys. Commun.* 191 (2015), p. 159. DOI: 10.1016/j.cpc.2015.01.024. arXiv: 1410.3012 [hep-ph].

[24] J. de Favereau et al. "DELPHES 3, A modular framework for fast simulation of a generic collider experiment". In: *JHEP* 02 (2014), p. 057. DOI: 10.1007/JHEP02(2014)057. arXiv: 1307.6346 [hep-ex].

[25] *The FCC Tutorials - FCC Tutorials documentation*. URL: https://hep-fcc.github.io/fcc-tutorials/main/index.html.

[26] Danilo Piparo et al. "RDataFrame: Easy Parallel ROOT Analysis at 100 Threads". In: *EPJ Web Conf.* 214 (2019). Ed. by A. Forti et al., p. 06029. DOI: 10.1051/epjconf/201921406029.

[27] Giacomo Polesello, Juliette Alimena, and Rebeca Gonzalez Suarez. *BSM Working Group Meeting*. URL: https://indico.cern.ch/event/1508638/#2-news.

[28] Ciaran O'Hare. *cajohare/AxionLimits: AxionLimits*. https://cajohare.github.io/AxionLimits/. Version v1.0. July 2020. DOI: 10.5281/zenodo.3932430.

Acknowledgments

I would like to thank Freya Blekman for giving me the opportunity to write my bachelor's thesis within the CMS group at DESY and for continuously encouraging me to step out of my comfort zone. She was the first person to expose me to the scientific research field by offering me a student assistant position in the CMS group - though, amusingly, due to a misunderstanding, she initially thought I was looking to write a bachelor's thesis. Fast forward one year, and I actually did end up writing my thesis in the group. Besides that, Freya is the first female scientist I truly ever looked up to. She has had a big impact on my still on-going journey, and I am very grateful for that.

I also want to show my heartfelt gratitude to Juliette Alimena who immediately made me feel welcome and was always incredibly understanding. She showed me that science is not just about numbers but also about people. Despite her busy schedule, she always made sure to find time to supervise, guide, and help me with the thesis. I am grateful for her regular and detailed feedback, which allowed me to aim for the best possible version of my work.

Special thanks go to Lovisa Rygaard for allowing me to distract her from her PhD work, for always answering my endless questions with patience, and for guiding me through the entire process. Her support throughout the past months made a significant difference, and I am very grateful for having had such an amazing office partner.

Lastly, I would like to express gratitude to my family and dear friends, who have shaped the past 21 years of my life and whose love and support made every success in life truly meaningful.

Appendix A: Produced signal samples

List of all produced signal samples for the sensitivity analysis conducted in Section 5.
1 000 000 events were generated for each sample. N_{exp} is the number of expected signal events for the Z-pole run before any selections are applied, N_{sel} represents the expected number of events after all event selections from Table 3 are applied and s is the sensitivity calculated with equation 8

m_a [GeV]	$c_{\gamma\gamma}$	N_{exp}	N_{sel}	s
1.0	1.0	2.75e+08	2.26e+08	1.27e+04
30.0	1.6	5.00e+08	1.58e+07	1.52e+03
10.0	1.6	6.79e+08	4.25e+08	1.87e+04
3.0	1.6	7.02e+08	5.67e+08	2.21e+04
1.0	1.6	7.04e+08	5.78e+08	2.23e+04
0.3	1.6	7.05e+08	5.31e+08	2.13e+04
0.1	1.6	7.05e+08	2.68e+08	1.41e+04
0.03	1.6	7.05e+08	1.98e+07	1.88e+03
0.01	1.6	7.05e+08	1.12e+05	1.17e+01
30.0	0.4	3.12e+07	9.95e+05	1.03e+02
10.0	0.4	4.25e+07	2.66e+07	2.45e+03
3.0	0.4	4.39e+07	3.54e+07	3.14e+03
1.0	0.4	4.40e+07	3.62e+07	3.20e+03
0.3	0.4	4.40e+07	3.32e+07	2.97e+03
0.1	0.4	4.40e+07	1.29e+07	1.26e+03
0.03	0.4	4.40e+07	8.85e+04	9.24e+00
0.01	0.4	4.40e+07	1.76e+02	1.84e-02
30.0	0.1	1.95e+06	6.21e+04	6.49e+00
10.0	0.1	2.65e+06	1.66e+06	1.72e+02
3.0	0.1	2.74e+06	2.21e+06	2.28e+02
1.0	0.1	2.75e+06	2.26e+06	2.33e+02
0.3	0.1	2.75e+06	2.03e+06	2.10e+02
0.1	0.1	2.75e+06	1.22e+05	1.27e+01
0.03	0.1	2.75e+06	3.25e+02	3.40e-02
0.01	0.1	2.75e+06	0.00e+00	1.51e-03
30.0	0.03	1.76e+05	5.56e+03	5.81e-01
10.0	0.03	2.39e+05	1.49e+05	1.56e+01
3.0	0.03	2.47e+05	1.99e+05	2.08e+01
1.0	0.03	2.48e+05	2.03e+05	2.12e+01
0.3	0.03	2.48e+05	1.14e+05	1.19e+01
0.1	0.03	2.48e+05	1.04e+03	1.09e-01
0.03	0.03	2.48e+05	2.48e+00	2.59e-04
0.01	0.03	2.48e+05	0.00e+00	2.62e-04

m_a [GeV]	$c_{\gamma\gamma}$	N_{exp}	N_{sel}	s
30.0	0.009	1.58e+04	5.05e+02	5.28e-02
10.0	0.009	2.15e+04	1.35e+04	1.41e+00
3.0	0.009	2.22e+04	1.79e+04	1.87e+00
1.0	0.009	2.23e+04	1.83e+04	1.91e+00
0.3	0.009	2.23e+04	1.52e+03	1.59e-01
0.1	0.009	2.23e+04	8.47e+00	8.85e-04
0.03	0.009	2.23e+04	6.69e-02	6.99e-06
30.0	0.002	7.81e+02	2.49e+01	2.60e-03
10.0	0.002	1.06e+03	6.65e+02	6.95e-02
3.0	0.002	1.10e+03	8.85e+02	9.25e-02
1.0	0.002	1.10e+03	4.92e+02	5.14e-02
0.3	0.002	1.10e+03	3.84e+00	4.01e-04
0.1	0.002	1.10e+03	2.75e-02	2.87e-06
30.0	0.0007	9.56e+01	3.07e+00	3.21e-04
10.0	0.0007	1.30e+02	8.15e+01	8.51e-03
3.0	0.0007	1.34e+02	1.09e+02	1.14e-02
1.0	0.0007	1.35e+02	1.03e+01	1.08e-03
0.3	0.0007	1.35e+02	5.41e-02	5.65e-06
0.1	0.0007	1.35e+02	2.70e-04	2.82e-08
30.0	0.0002	7.81e+00	2.48e-01	2.59e-05
10.0	0.0002	1.06e+01	6.69e+00	6.99e-04
3.0	0.0002	1.10e+01	4.52e+00	4.72e-04
1.0	0.0002	1.10e+01	7.07e-02	7.39e-06
0.3	0.0002	1.10e+01	3.30e-04	3.45e-08
30.0	0.00005	4.88e-01	1.55e-02	1.62e-06
10.0	0.00005	6.63e-01	4.53e-01	4.73e-05
3.0	0.00005	6.86e-01	2.41e-02	2.52e-06
1.0	0.00005	6.88e-01	2.65e-04	2.77e-08
30.0	0.00001	1.95e-02	5.66e-04	5.91e-08
10.0	0.00001	2.65e-02	4.14e-03	4.32e-07
3.0	0.00001	2.74e-02	3.80e-05	3.97e-09
30.0	0.000004	3.12e-03	7.02e-05	7.33e-09
10.0	0.000004	4.25e-03	1.17e-04	1.22e-08
3.0	0.000004	4.39e-03	9.26e-07	3.97e-09
30.0	0.000001	1.95e-04	9.48e-07	9.90e-11
10.0	0.000001	2.65e-04	4.74e-07	4.95e-11

Appendix B: MadGraph process card

```
#************************************************************
#*                     MadGraph5_aMC@NLO                    *
#*                                                          *
#*                *                       *                 *
#*                  *        * *        *                   *
#*                    * * * * 5 * * * *                     *
#*                  *        * *        *                   *
#*                *                       *                 *
#*                                                          *
#*                                                          *
#*         VERSION 3.2.0                 2021-08-22         *
#*                                                          *
#*    The MadGraph5_aMC@NLO Development Team - Find us at   *
#*    https://server06.fynu.ucl.ac.be/projects/madgraph     *
#*                                                          *
#************************************************************
#*                                                          *
#*               Command File for MadGraph5_aMC@NLO         *
#*                                                          *
#*     run as ./bin/mg5_aMC  filename                       *
#*                                                          *
#************************************************************
set group_subprocesses Auto
set ignore_six_quark_processes False
set low_mem_multicore_nlo_generation False
set complex_mass_scheme False
set include_lepton_initiated_processes False
set gauge unitary
set loop_optimized_output True
set loop_color_flows False
set max_npoint_for_channel 0
set default_unset_couplings 99
set max_t_for_channel 99
set zerowidth_tchannel True
set nlo_mixed_expansion True
set auto_convert_model T
import model sm
define p = g u c d s u~ c~ d~ s~
define j = g u c d s u~ c~ d~ s~
define l+ = e+ mu+
define l- = e- mu-
define vl = ve vm vt
define vl~ = ve~ vm~ vt~
import model ALP_NLO_UFO
generate e+ e- > Z, (Z > a ALP, (ALP > a a))
output /eos/user/e/ebakhish/MG/MGOutput/ALP_Z_aa_3p0GeV_cYY1p0/ALP_Z_aa_3p0GeV_cYY1p0_0
launch /eos/user/e/ebakhish/MG/MGOutput/ALP_Z_aa_3p0GeV_cYY1p0/ALP_Z_aa_3p0GeV_cYY1p0_0
done
# set to electron beams (0 for ele, 1 for proton)
set lpp1 0
set lpp2 0
set ebeam1 45.594
set ebeam2 45.594
```

```
# set to electron beams (0 for ele, 1 for proton)
set lpp1 0
set lpp2 0
set ebeam1 45.594
set ebeam2 45.594
# set ALP mass
set Ma 3.0
# set ALP couplings
set cWW = 0.0
set CYY = 1.0
set cGG = 0.
set cuu = 0.
set cdd = 0.
set ccc = 0.
set css = 0.
set ctt = 0.
set cbb = 0.
set cee = 0.
set cmumu = 0.
set ctautau = 0.
set cah = 0.
set cZh5 = 0.
# set supression scale in the effective operators coupling the ALP to SM particles: 1000/(16*pi**2)
set falp = 6.33

# set the decay width of the ALP to auto
set WALP auto
set time_of_flight 0
set nevents 1000000
set iseed 28250
done
```

Appendix C: Pythia process card

```
! File: ALP_pythia.cmd
Random:setSeed = on
Main:timesAllowErrors = 10         ! how many aborts before run stops
Main:numberOfEvents = 1000000         ! number of events to generate


! 2) Settings related to output in init(), next() and stat().
Next:numberCount = 100             ! print message every n events
!Beams:idA = 11                     ! first beam, e+ = 11
!Beams:idB = -11                    ! second beam, e- = -11

Beams:frameType = 4                ! read info from a LHEF
! Change the LHE file here
!Beams:LHEF = /eos/experiment/fcc/ee/analyses_storage/BSM/LLPs/ALPs_3photons/mg5amcnlo/madgraph_5_1.0/Events/run_01/unweighted_events.lhe
Beams:LHEF = /eos/user/e/ebakhish/MG/MGOutput/ALP_Z_aa_3p0GeV_cYY1p0/ALP_Z_aa_3p0GeV_cYY1p0_0/Events/run_01/unweighted_events.lhe.gz


! 3) Settings for the event generation process in the Pythia8 library.
PartonLevel:ISR = on               ! initial-state radiation
PartonLevel:FSR = on               ! final-state radiation

LesHouches:setLifetime = 2
```

Appendix D: MadGraph *run_card.dat*

```
#*********************************************************************
# Standard Cuts                                                      *
#*********************************************************************
# Minimum and maximum pt's (for max, -1 means no cut)                *
#*********************************************************************
 10.0  = pta       ! minimum pt for the photons
 -1.0  = ptamax    ! maximum pt for the photons
 {} = pt_min_pdg ! pt cut for other particles (use pdg code). Applied on particle and anti-particle
 {} = pt_max_pdg ! pt cut for other particles (syntax e.g. {6: 100, 25: 50})
#*********************************************************************
# Minimum and maximum E's (in the center of mass frame)              *
#*********************************************************************
  0.0  = ej     ! minimum E for the jets
  0.0  = eb     ! minimum E for the b
  0.0  = ea     ! minimum E for the photons
  0.0  = el     ! minimum E for the charged leptons
  -1.0   = ejmax ! maximum E for the jets
 -1.0   = ebmax ! maximum E for the b
 -1.0   = eamax ! maximum E for the photons
 -1.0   = elmax ! maximum E for the charged leptons
 {} = e_min_pdg ! E cut for other particles (use pdg code). Applied on particle and anti-particle
 {} = e_max_pdg ! E cut for other particles (syntax e.g. {6: 100, 25: 50})

#*********************************************************************
# Maximum and minimum absolute rapidity (for max, -1 means no cut)   *
#*********************************************************************
 2.5  = etaa    ! max rap for the photons
 0.0  = etajmin ! min rap for the jets
 0.0  = etaamin ! min rap for the photons
 {} = eta_min_pdg ! rap cut for other particles (use pdg code). Applied on particle and anti-particle
 {} = eta_max_pdg ! rap cut for other particles (syntax e.g. {6: 2.5, 23: 5})
#*********************************************************************
# Minimum and maximum DeltaR distance                                *
#*********************************************************************
 0.4 = draa    ! min distance between gammas
 -1.0  = draamax ! max distance between gammas
#*********************************************************************
# Minimum and maximum invariant mass for pairs                       *
#*********************************************************************
 0.0   = mmaa    ! min invariant mass of gamma gamma pair
 -1.0  = mmaamax ! max invariant mass of gamma gamma pair
 {} = mxx_min_pdg ! min invariant mass of a pair of particles X/X~ (e.g. {6:250})
 {'default': False} = mxx_only_part_antipart ! if True the invariant mass is applied only
                      ! to pairs of particle/antiparticle and not to pairs of the same pdg codes.
#*********************************************************************
```

Appendix E: IDEA card

```
642  ##################
643  # Photon efficiency
644  ##################
645
646  module Efficiency PhotonEfficiency {
647    set InputArray Calorimeter/eflowPhotons
648    set OutputArray photons
649
650    # set EfficiencyFormula {efficiency formula as a function of eta and pt}
651    # efficiency formula for photons
652    set EfficiencyFormula {
653          (energy < 2.0)                                          * (0.000)+
654          (energy >= 2.0) * (abs(eta) <= 0.88)                    * (0.99) +
655          (energy >= 2.0) * (abs(eta) >0.88 && abs(eta) <= 3.0) * (0.99) +
656          (abs(eta) > 3.0)                                        * (0.000)
657    }
658  }
659
```

```
702  ####################
703  # Electron efficiency
704  ####################
705
706  module Efficiency ElectronEfficiency {
707    set InputArray ElectronFilter/electrons
708    set OutputArray electrons
709
710    # set EfficiencyFormula {efficiency formula as a function of eta and pt}
711
712    # efficiency formula for electrons
713    set EfficiencyFormula {
714          (energy < 2.0)                                          * (0.000)+
715          (energy >= 2.0) * (abs(eta) <= 0.88)                    * (0.99) +
716          (energy >= 2.0) * (abs(eta) >0.88 && abs(eta) <= 3.0)  * (0.99) +
717          (abs(eta) > 3.0)                                        * (0.000)
718    }
719  }
720
```

Statutory Declaration

I declare that I have authored the Bachelor's thesis independently and have not used any aids other than those specified. I have clearly labeled all passages that are taken from other works in terms of wording or meaning as borrowed material, stating the exact source in each case. I confirm that I have not already submitted this thesis in the same or a similar version in another examination procedure. If electronic aids based on generative artificial intelligence (gAI) were used in the course of the preparation of this Bachelor's thesis, I confirm that my own work was the main focus and that complete documentation of all aids used is available in accordance with good scientific practice. I am responsible for any incorrect or distorted content, incorrect references, violations of data protection and copyright law or plagiarism generated by the gAI.
I agree that the Bachelor's thesis may be published.

Place, date Hamburg, 19.03.2025 Signature: